A supersymmetric model for lattice fermions

Huijse, L.

Chapter 4
The supersymmetric model on the one dimensional chain

4.1 Introduction

In this chapter we discuss the supersymmetric model on the one dimensional chain. The supersymmetric model was first introduced for this lattice [22]. Its ground state structure was investigated and the model was foud to be integrable and solved via Bethe Ansatz. The continuum limit is described by an $\mathcal{N} = (2,2)$ superconformal field theory with central charge $c = 1$. In follow up work, a precise mapping of this model onto the antiferromagnetic critical XXZ Heisenberg spin chain was presented [23] and the chain with open boundary conditions was investigated, both analytically and numerically [51].
Here we will not only briefly review these results, but we will also present a detailed analysis relating the lattice model spectrum and operators to the operator content of the continuum theory. We will see that this model forms a textbook example of how a superconformal field theory can be identified studying the finite size lattice model properties. Apart from finite size scaling of the spectrum, we will study a boundary twist, one-point functions and entanglement entropy. The boundary twist in the lattice model is related to a spectral flow in the continuum theory. The power of this type of analysis is that it does not require a comparison between models on lattices with different size (length). This will prove very useful in chapter 7.

4.2 Hamiltonian

For convenience, we restate the hamiltonian for the supersymmetric model on the one dimensional periodic chain of length L:

$$\begin{aligned} H = \{Q^\dagger, Q\} &= \sum_i \sum_{j \text{ next to } i} P_{<i>} c_i^\dagger c_j P_{<j>} + \sum_i P_{<i>} \\ &= \sum_{i=1}^{L} \Big[P_{i-1} \big(c_i^\dagger c_{i+1} + c_{i+1}^\dagger c_i \big) P_{i+2} \Big] + \sum_{i=1}^{L} (n_i n_{i+2}) + L - 2F. \end{aligned}$$

Here $P_i = 1 - n_i$, $n_i = c_i^\dagger c_i$ is the usual number operator and $F = \sum_i n_i$ is the total number of fermions.

4.3 Witten index

In the example of the 6-site chain (section 2.1.4) we saw that the Witten index can be computed by simply summing over all possible configurations with the appropriate sign. However, because of the hard-core character of the fermions this is not a trivial problem

for larger sizes. To compute the Witten index for chains of arbitrary length we use the following method [22]. First divide the lattice into two sublattices S_1 and S_2. Then fix the configuration on S_1 and sum $(-1)^F$ for the configurations on S_2. Finally, sum the results over the configurations of S_1. Of course the trick is to make a smart choice for the sublattices. For the periodic chain with $L = 3j$ sites, we take S_2 to be every third site. All the sites on S_2 are disconnected and thus every site can be either empty or occupied given that its neighboring sites on S_1 are empty. This means that the sum of $(-1)^F$ for the configurations on S_2 vanishes as soon as at least one site on S_2 can be both empty and occupied. Consequently, the only non-zero contribution comes from the configurations such that at least one of the adjacent sites on S_1 is occupied for each site on S_2. There are only two such configurations:

$$\begin{aligned} |\alpha\rangle &\equiv \cdots \bullet \square \circ \bullet \square \circ \bullet \square \circ \bullet \square \circ \bullet \square \circ \bullet \square \circ \bullet \square \circ \ldots \\ |\gamma\rangle &\equiv \cdots \circ \square \bullet \circ \square \bullet \circ \square \bullet \circ \square \bullet \circ \square \bullet \circ \square \bullet \circ \square \bullet \ldots \end{aligned} \tag{4.1}$$

where the square represents an empty site on S_2. The final step is to sum $(-1)^F$ for these two configurations, and since both configurations have $f = L/3 = j$, we find that the Witten index is $W = 2(-1)^j$. Note that this agrees with the result we obtained for the 6-site chain. One can also use this method of splitting the lattice in sublattices to compute the cohomology, i.e. the total number of ground states. We will come back to this in section 4.4. First, however, we discuss a different method to compute the Witten index that nicely generalizes to arbitrary chain lengths and open boundary conditions.

4.3.1 Transfer matrix

There is an alternative way of computing the Witten index by using the transfer matrix. Let us write the partition function as

$$Z = \sum_{\text{states}} z^f e^{-\beta E}, \tag{4.2}$$

where $z \equiv e^{\beta\mu}$ is the fugacity, β is the inverse temperature, μ is the chemical potential and E and f are the energy and fermion number, respectively. If we take the limit where $\beta E \to 0$, but $\beta\mu$ finite, the partition function becomes an important combinatorial tool. In this limit we obtain

$$Z(z) = \sum_{\text{states}} z^f. \tag{4.3}$$

It follows that $Z(z = 1)$ is the size of the Hilbert space. More importantly, $Z(z = -1)$ is precisely the Witten index. Remember that because of the nearest neighbor exclusion rule, the occupation number n_i of a site i depends on the occupation numbers of the neighboring sites. It follows that we can write the partition function of a periodic chain of L sites as

$$Z(z) = \sum_{\text{states}} z^f = \sum_{\text{states}} \prod_i z^{n_i} = \text{Tr } \mathcal{T}^L, \tag{4.4}$$

where $\mathcal{T}$ is the transfer matrix given by

$$\mathcal{T}_{ij} = (1 - \delta_{2,n_i+n_j}) z^{n_i} \Rightarrow \mathcal{T} = \begin{pmatrix} 1 & 1 \\ z & 0 \end{pmatrix}$$

where we chose the basis $n_1 = 0$ and $n_2 = 1$. The eigenvalues of the transfer matrix are $\frac{1}{2} \pm \frac{1}{2}\sqrt{1+4z}$. From this we obtain the following expression for the Witten index for a periodic chain of L

$$W = Z(z=-1) = (\frac{1}{2} + \frac{1}{2}\imath\sqrt{3})^L + (\frac{1}{2} - \frac{1}{2}\imath\sqrt{3})^L. \tag{4.5}$$

Rewriting this we get

$$W = e^{\pi\imath L/3} + e^{-\pi\imath L/3} = 2\cos(\pi L/3). \tag{4.6}$$

For $L \mod 6 = 0, 1, 2, 3, 4, 5$ we find $W = 2, 1, -1, -2, -1, 1$ respectively.
One can also obtain the Witten index for open boundary conditions. In that case, the first and last site both have just one neighbor and the partition function can be written as

$$Z(z) = \sum_{i,j=1}^{2} (\mathcal{T}^{L-1})_{ij} c_j, \tag{4.7}$$

where $c_1 = 1$ and $c_2 = z$. One can verify that this gives

$$W = -\frac{2}{\sqrt{3}} \sin(\pi(L-1)/3). \tag{4.8}$$

It follows that for the chain with open boundary conditions with length $L \mod 6 = 0, 1, 2, 3, 4, 5$ the Witten index is $W = 1, 0, -1, -1, 0, 1$ respectively. Clearly, the transfer matrix is a very powerful tool to obtain the Witten index.

4.3.2 Ground state momenta

For the periodic chain the hamiltonian commutes with the translation operator T. A nice way to compute the momenta of the ground states of the periodic chain, is to compute the Witten index per momentum sector, characterized by the eigenvalues of T [23]. Unfortunately, there is not an obvious way to do this for general system size. For small system sizes, however, it is a very simple computation. One writes down all configurations modulo translations, determines the possible eigenvalues of T for each configuration and computes the Witten index per sector. The procedure is illustrated for the 6-site chain in table 4.1. One easily reads off that the Witten index is unity in the momentum sectors with translation eigenvalues $t = e^{\pi\imath/3}$ and $t = e^{5\pi\imath/3}$. The two zero energy ground states of the 6-site periodic chain thus have momenta $\pi/3$ and $5\pi/3$.
By doing this computation for various small system sizes one can figure out the systematics. It was found that [23] for periodic chains of length $L = 3j$ the Witten index W_t at fixed translation eigenvalue t reads

$$W_t = \begin{cases} (-1)^L & \text{for } t = (-1)^{L+1} e^{2\pi\imath k/3} \text{ with } k = 1, 2 \\ 0 & \text{otherwise,} \end{cases} \tag{4.9}$$

and for all other lengths L

$$W_t = \begin{cases} (-1)^{L+1} & \text{for } t = (-1)^{L+1} \\ 0 & \text{otherwise.} \end{cases} \tag{4.10}$$

Table 4.1: We show the procedure to compute the Witten index per momentum sector for the 6-site chain. In the first column we show the possible configurations modulo translation for the 6-site chain. We use the notation where we write $c_1^\dagger c_3^\dagger|0\rangle$ for example as $|101000\rangle$, so that the translation eigenvalues can easily be read of. In the second column, we show the possible eigenvalues t_k of the translation operator T in terms of k, where $t_k = e^{\pi\imath k/3}$. In columns 3 through 8, we give $(-1)^F$ for the different configurations. If a configuration does not occur in a given sector we write a zero. Finally, in the bottom row, we compute the Witten index in the momentum sectors corresponding to $k = 1, \ldots, 6$ by adding the entries in columns 3 through 8. That is, we compute $W_k = \mathrm{Tr}_k(-1)^F$, where the trace is restricted to states with translation eigenvalue t_k.

configurations "mod T"	eigenvalues of T: possible values of k for $t_k = e^{\pi\imath k/3}$	$(-1)^F$ for $k=1$	$(-1)^F$ for $k=2$	$(-1)^F$ for $k=3$	$(-1)^F$ for $k=4$	$(-1)^F$ for $k=5$	$(-1)^F$ for $k=6$
$\|000000\rangle$	$t^1 = 1 \Rightarrow k = 6$	0	0	0	0	0	1
$\|100000\rangle$	$t^6 = 1 \Rightarrow k = 1, \ldots, 6$	-1	-1	-1	-1	-1	-1
$\|101000\rangle$	$t^6 = 1 \Rightarrow k = 1, \ldots, 6$	1	1	1	1	1	1
$\|100100\rangle$	$t^3 = -1 \Rightarrow k = 1, 3, 5$	1	0	1	0	1	0
$\|101010\rangle$	$t^2 = 1 \Rightarrow k = 3, 6$	0	0	-1	0	0	-1
Witten index per sector:		1	0	0	0	1	0

4.4 Cohomology

To find the exact number of ground states we compute the cohomology by using the 'tic-tac-toe' lemma of [33] (see section 2.2.3). This says that under certain conditions, the cohomology H_Q for $Q = Q_1 + Q_2$ is the same as the cohomology of Q_1 acting on the cohomology of Q_2. In an equation, $H_Q = H_{Q_1}(H_{Q_2}) \equiv H_{12}$, where Q_1 and Q_2 act on different sublattices S_1 and S_2. We find H_{12} by first fixing the configuration on all sites of the sublattice S_1, and computing the cohomology H_{Q_2}. Then one computes the cohomology of Q_1, acting not on the full space of states, but only on the classes in H_{Q_2}. A sufficient condition for the lemma to hold is that all non-trivial elements of H_{12} have the same f_2 (the fermion-number on S_2). For the periodic chain with $L = 3j$ we choose the sublattice as before (see section 4.3: S_2 is every third site). Now consider a single site on S_2. If both of the adjacent S_1 sites are empty, H_{Q_2} is trivial: Q_2 acting on the empty site does not vanish, while the filled site is Q_2 acting on the empty site. Thus H_{Q_2} is non-trivial only when every site on S_2 is forced to be empty by being adjacent to an occupied site. The elements of H_{Q_2} are just the two states $|\alpha\rangle$ and $|\gamma\rangle$ pictured above in equation (4.1). Both states $|\alpha\rangle$ and $|\gamma\rangle$ belong to H_{12}: they are closed because $Q_1|\alpha\rangle = Q_1|\gamma\rangle = 0$, and not exact because there are no elements of H_{Q_2} with $f_1 = f - 1$. By the tic-tac-toe lemma, there must be precisely two different cohomology classes in H_Q, and therefore exactly two ground states with $f = L/3$. Applying the same arguments to the periodic chain with $3j \pm 1$ sites and to the open chain yields in all cases exactly one $E = 0$ ground state, except in open chains with $3j + 1$ sites, where there are none [23] (see also section 6.3).

4.5 Bethe Ansatz solution in continuum limit

The supersymmetric model on the chain can be solved exactly through a Bethe Ansatz [22]. In the continuum limit one can derive the thermodynamic Bethe Ansatz equations. The model has the same thermodynamic equations as the XXZ Heisenberg spin chain at a specific value of the anisotropy parameter Δ. There is indeed a mapping between the supersymmetric model on the chain and the Heisenberg spin chain with special boundary conditions [23]. The hamiltonian of the XXZ chain is defined in terms of the usual Pauli matrices as

$$H_{\mathrm{XXZ}} = \frac{1}{2}\sum_{i=1}^{L}\left[\sigma_i^x\sigma_{i+1}^x + \sigma_i^y\sigma_{i+1}^y - \Delta\sigma_i^z\sigma_{i+1}^z\right]. \tag{4.11}$$

The continuum limit of the XXZ chain is described by the massless Thirring model [52], or equivalently a free massless boson Φ with action [53]

$$S = \frac{g}{4\pi}\int dx\,dt\ \left[(\partial_t\Phi)^2 - (\partial_x\Phi)^2\right]. \tag{4.12}$$

The coupling constant g is related to the anisotropy parameter Δ in the XXZ chain. On the conformal field theory side the coupling constant g is related to the compactification radius R of the free boson theory via $g = 2/R^2$. The free boson theory is characterized by a central charge $c = 1$ and a set of highest weight states which depend on the compactification radius. At a compactification radius $R = \sqrt{3}$, the conformal algebra is enhanced to an $\mathcal{N} = (2,2)$ superconformal algebra [54, 53]. The $(2,2)$ means that both the holomorphic as well as the anti-holomorphic fields satisfy an $\mathcal{N} = 2$ superconformal algebra. More specifically, the free boson at compactification radius $R = \sqrt{3}$ is the simplest field theory with $\mathcal{N} = (2,2)$, namely the first in the series of minimal supersymmetric models. It turns out that the compactification radius $R = \sqrt{3}$ corresponds to an anisotropy parameter of $\Delta = -1/2$ (see for example [55]) which is precisely the value one obtains upon mapping the supersymmetric model onto the XXZ chain.
The fact that the low-energy spectrum of the supersymmetric model on the chain is described by a superconformal theory in the continuum limit, tells us that the model is quantum critical.

4.6 Relation to other models

Before we explore the continuum limit of the supersymmetric model on the chain in great detail in the following sections, we would like to mention the relation between this model and three other models. The models are, firstly, a generalization of the supersymmetric model discussed here [23], secondly, the XXZ Heisenberg spin chain, a famous integrable model without explicit supersymmetry, and finally, the supersymmetric matrix model [56] at strong coupling, an explicitly supersymmetric model that arose as a toy-model in the context of high energy physics. Both our supersymmetric model on the chain as well as the supersymmetric matrix model in the strong coupling limit can be mapped explicitly onto the XXZ Heisenberg spin chain [23, 57], making the models equivalent under certain conditions.

4.6.1 A family of supersymmetric models

In [23] a generalization of the supersymmetric model was presented, generating a whole family of supersymmetric lattice models. Interestingly, all these models can be tuned to be quantum critical. The lattice models can be labelled by an index k and it was shown that in the continuum limit their low-energy spectrum is described by the k-th superconformal field theory in the minimal series (see section 3.4). The generalization follows from allowing no more than k consecutive sites to be occupied on the chain. Clearly, the supersymmetric model discussed in this chapter has $k = 1$. For the model with $k = 1$ we can define the supercharge Q as a sum over the hard-core fermion creation operators $d_i^\dagger \equiv P_{i-1}c_i^\dagger P_{i+1}$. For $k = 2$ a second type of creation operator $e_i^\dagger \equiv P_{i-2}c_{i-1}^\dagger c_{i-1}c_i^\dagger P_{i+1} + P_{i-1}c_i^\dagger c_{i+1}^\dagger c_{i+1}P_{i+2}$ is introduced, which creates a particle on site i if precisely one of its neighbors is occupied and both neighbors of the occupied site are empty. The supercharge Q is now defined as

$$Q = \sum_i [y_1 d_i^\dagger + y_2 e_i^\dagger].$$

The nilpotency condition of the supercharges is satisfied for all values of y_1 and y_2, so the ratio $x_1 = y_1/y_2$ is a non-trivial adjustable parameter in the model. The quantum critical point is reached by setting $x_1 = \sqrt{2}$. For general k the supersymmetric model can be constructed in a similar manner and has $k-1$ adjustable parameters. For further details and a full analysis of these models we refer to [23].

4.6.2 The XXZ Heisenberg spin chain

The hamiltonian of the XXZ Heisenberg spin chain is given in (4.11). The mapping can be found in detail in [23] (see also [58]), here we will sketch the main idea. To map the supersymmetric model onto a spin chain, we identify a site, occupied by a fermion, including its adjacent edges with a down-spin and an edge between two empty sites with an up-spin (see figure 4.1). The length L of the spin chain can therefore be written as $L = N - f$, where N is the length of the original fermion chain and f is the number of fermions. From this map one finds that a fermion that hops from one site to the next, corresponds to a spin flip between two neighboring spins. More precisely, we find

$$\begin{gathered} \textstyle\sum_i \left[P_{i-1}\left(c_i^\dagger c_{i+1} + c_{i+1}^\dagger c_i\right)P_{i+2}\right] \\ \Longleftrightarrow \\ \textstyle\sum_j \left[\sigma_j^+\sigma_{j+1}^- + \sigma_j^-\sigma_{j+1}^+\right] \end{gathered}$$

where the spin-flip operators are defined in terms of the usual Pauli matrices, $\sigma^\pm \equiv (\sigma^x \pm \imath\sigma^y)/2$. The diagonal term in the supersymmetric hamiltonian counts the number of empty next-nearest neighbor pairs. Under the mapping such a pair either translates into a down-spin or into a pair of neighboring up-spins. We thus find

$$\sum_i P_{<i>} \Longleftrightarrow \sum_j (1-\sigma_j^z)/2 + (1+\sigma_j^z)(1+\sigma_{j+1}^z)/4. \tag{4.13}$$

Working out the latter for a periodic spin chain, we find $(3L + \sum_j \sigma_j^z\sigma_{j+1}^z)/4$. Combining the results for the diagonal and off-diagonal terms we find that the supersymmetric model

maps onto the XXZ Heisenberg spin chain up to an additive constant

$$H_{\text{SUSY}} = \sum_{i=1}^{N} \left[P_{i-1} \left(c_i^\dagger c_{i+1} + c_{i+1}^\dagger c_i \right) P_{i+2} + P_{<i>} \right]$$
$$\Longleftrightarrow$$
$$H_{\text{XXZ}} + \tfrac{3L}{4} = \tfrac{1}{2} \sum_{j=1}^{L} \left[\sigma_j^x \sigma_{j+1}^x + \sigma_j^y \sigma_{j+1}^y + \tfrac{1}{2} \sigma_j^z \sigma_{j+1}^z \right] + \tfrac{3L}{4} \quad .$$

Note that since $L = N - f$, the supercharges do note preserve the length of the spin chain. This explains why supersymmetry is not explicit in the spin chain. Furthermore, note that the supersymmetric model maps unto the XXZ spin chain with anisotropy parameter $\Delta = -1/2$ (4.11).

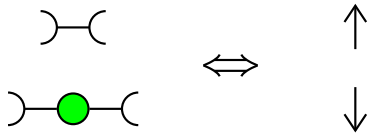

Figure 4.1: To map the supersymmetric model onto a spin chain, we identify an edge between two empty sites (top left) with an up-spin (top right) and a site, occupied by a fermion, including its adjacent edges (bottom left) with a down-spin (bottom right).

In spite of this mapping, the two hamiltonians do not have entirely the same spectrum when periodic boundary conditions are imposed (for open boundary conditions these subtleties do not occur and the two spectra are indeed equal). It turns out that for periodic boundary conditions the sizes of the Hilbert spaces at corresponding sectors do not agree due to an ambiguity in the mapping. Furthermore, due to the anti-commutation relations satisfied by the fermions, a state acquires a minus sign when a fermion hops over the boundary in a state with an even number of fermions. These differences can be overcome by restricting to sectors with translation eigenvalue t and introducing twisted boundary conditions in the spin chain (for details see [23]).

4.6.3 A supersymmetric matrix model

In a series of papers [56, 59, 57] Veneziano and Wosiek introduce and investigate a supersymmetric matrix model. The model was introduced in the context of high energy physics, where it was proposed as a toy model to study a claimed equivalence [60] between a non-supersymmetric theory, such as quantum chromo dynamics, and a supersymmetric "parent" theory. It turns out, however, that the model is quite interesting in its own right. In particular, investigations of the model in a special limit independently led to the observation that the XXZ Heisenberg spin chain has a hidden supersymmetry at $\Delta = -1/2$ [57]. This observation followed from an explicit mapping to the spin chain. Since both the supersymmetric model discussed in this thesis as well as the supersymmetric matrix model, can be mapped to the XXZ spin chain, there may be a direct relation between the two. Exploiting this relation may lead to further insights for both models.
In a matrix model the usual quantum mechanical creation and annihilation operators for bosons and fermions are replaced by $N \times N$ matrices. It follows that there are N^2 bosonic and N^2 fermionic degrees of freedom. The usual (anti-)commutation relations are replaced by

$$\begin{aligned} [a_{ij}, a_{kl}^\dagger] &= \delta_{jk}\delta_{il} \quad \text{for the bosons and} \\ \{f_{ij}, f_{kl}^\dagger\} &= \delta_{jk}\delta_{il} \quad \text{for the fermions.} \end{aligned}$$

Veneziano and Wosiek choose to define the supercharges as

$$Q = \mathrm{Tr}[fa^\dagger(1+ga^\dagger)], \quad Q^\dagger = \mathrm{Tr}[f^\dagger a(1+ga)] \tag{4.14}$$

and the hamiltonian reads

$$H = \{Q^\dagger, Q\}. \tag{4.15}$$

Note that the hamiltonian conserves the number of fermions $F = \mathrm{Tr}(f^\dagger f)$, whereas, is can change the number of bosons $B = \mathrm{Tr}(a^\dagger a)$ by 0,1 or -1.
The model is studied in the large N limit. In the limit of $N \to \infty$, while keeping the 't Hooft coupling $\lambda = g^2 N$ fixed, the so-called single trace states

$$|n_1, \ldots, n_F\rangle = \mathrm{Tr}[(a^\dagger)^{n_1} f^\dagger \ldots (a^\dagger)^{n_F} f^\dagger]|0\rangle \tag{4.16}$$

are invariant under the action of the hamiltonian. The action of the hamiltonian on other states can be shown to generate terms which are subleading in N. The other states can thus simply be discarded in the large N limit, since the single-trace states form a closed subspace under the action of the hamiltonian.
In a remarkable series of papers [56, 59, 57] Veneziano and Wosiek show that this model is far from trivial. Since the hamiltonian conserves the total number of fermions, the model can be studied in sectors with fixed F. For the sectors with $F = 0, 1, 2, 3, 4$ various interesting analytical and numerical results were obtained. These results include Witten index computations as a function of the 't Hooft coupling, clear evidence of a phase transition at 't Hooft coupling $\lambda = 1$ accompanied by a jump in the Witten index (see also [61]), an exact strong-weak coupling duality and a mapping to the XXZ Heisenberg spin chain in the strong coupling limit. In [62] these results are extended with an analytic expression for the ground state in sectors with $F = 2, 4$, by computing the harmonic representatives of the cohomology of Q.
Let us briefly discuss the mapping to the XXZ Heisenberg spin chain (4.11). In the strong coupling limit, that is $\lambda \to \infty$, the hamiltonian reduces to H_{SC}, which conserves both F and B. Veneziano and Wosiek find the following relations [57]

- for F odd $H_{\mathrm{SC}} \Leftrightarrow H_{\mathrm{XXZ}} + \frac{3}{4}L$, with anisotropy parameter $\Delta = -\frac{1}{2}$,
- for F even and B odd $H_{\mathrm{SC}} \Leftrightarrow -H_{\mathrm{XXZ}} + \frac{3}{4}L$, with anisotropy parameter $\Delta = \frac{1}{2}$,
- for F *and* B even no equivalence was found.

The length of the spin chain is $L = F + B$ and the conserved component of the total spin is $S_z = \frac{1}{2}(F - B)$. Also here the spectrum on the spin side should be computed for fixed values of the translation eigenvalue.
These mappings suggest that there is a direct relation between the supersymmetric model on the chain and the supersymmetric matrix model in the strong coupling limit with F odd.

4.7 Free boson with $\mathcal{N} = (2, 2)$ supersymmetry

The continuum limit of the supersymmetric model on the chain is described by the free boson (4.12) with $\mathcal{N} = (2, 2)$ supersymmetry [22]. The supersymmetry arises as an enhanced symmetry for a specific compactification radius or, equivalently, a specific coupling

g. In this section we will discuss this theory in some detail and in particular its relation to the lattice model. Let us first see how the $\mathcal{N} = (2,2)$ supersymmetry arises at compactification radius $R = \sqrt{3}$, and thus $g = 2/3$.
The free boson field Φ can be decoupled into left and right movers: $\Phi = \Phi_L + \Phi_R$ and the dual is defined as $\tilde{\Phi} = g(\Phi_L - \Phi_R)$. The left moving field obeys the following OPEs

$$\Phi_L(z)\Phi_L(w) \sim -\frac{1}{2g}\ln(z-w), \quad \partial\Phi_L(z)\partial\Phi_L(w) \sim -\frac{1}{2g}\frac{1}{(z-w)^2},$$

and similarly for the right moving field

$$\Phi_R(\overline{z})\Phi_R(\overline{w}) \sim -\frac{1}{2g}\ln(\overline{z}-\overline{w}), \quad \partial\Phi_R(\overline{z})\partial\Phi_R(\overline{w}) \sim -\frac{1}{2g}\frac{1}{(\overline{z}-\overline{w})^2}.$$

The operators

$$V_{m,n} = :\exp(\imath m\Phi + \imath n\tilde{\Phi}):\,,$$

are called vertex operators. Here the semicolons imply normal ordering, in the following we will drop this notation and tacitly assume that normal ordering is taken care of. The vertex operators are primary fields (see (3.3)) and their conformal dimensions are

$$h_{L,R} = (m \pm gn)^2/(4g), \tag{4.17}$$

with $m \in \mathbb{Z}$ and $n \in \mathbb{Z}/2$. Note that we label holomorphic and anti-holomorphic dimensions with L and R, for left and right movers, respectively. Remember that in an $\mathcal{N} = 2$ superconformal field theory there are two supercharges of conformal dimension 3/2 and a $U(1)$ current of dimension 1. From (4.17) we find that for $R = \sqrt{3}$, and thus $g = 2/3$, the operators $V_{\pm1,\pm3/2}$ have conformal dimensions $(h_L, h_R) = (3/2, 0)$ and the operators $V_{\pm1,\mp3/2}$ have conformal dimensions $(h_L, h_R) = (0, 3/2)$. These four operators are the two left mover supercharges and two right mover supercharges. Finally, the $U(1)$ currents of dimensions $(1,0)$ and $(0,1)$ are proportional to $\partial\Phi_L$ and $\partial\Phi_R$ respectively. The proportionality factor follows from comparing the OPEs of $\partial\Phi_{L,R}$ with the OPE of the U(1) current (see (3.5))

$$J(z)J(w) \sim \frac{c/3}{(z-w)^2} \Rightarrow J_{L,R}(z) = \pm\imath\sqrt{2gc/3}\partial\Phi_{L,R} = \pm\imath 2/3\partial\Phi_{L,R}. \tag{4.18}$$

So these operators, together with the stress-energy tensor form an $\mathcal{N} = (2,2)$ superconformal algebra.

4.7.1 Spectrum

The spectrum of a superconformal field theory can be generated from the highest weight states by acting with the Virasoro generators and the supercharges. The effect of the Virasoro generators on a highest weight state $|h_L, h_R\rangle$ is well known

$$\begin{aligned}
L_{L,R;0}|h_L,h_R\rangle &= h_{L,R}|h_L,h_R\rangle,\\
L_{L,R;n}|h_L,h_R\rangle &= 0,\\
L_{L,-n}|h_L,h_R\rangle &= |h_L+n,h_R\rangle,\\
L_{R,-n}|h_L,h_R\rangle &= |h_L,h_R+n\rangle,
\end{aligned}$$

with $n > 0$. The vacuum is defined as the state with $L_{L,R;0}|0\rangle = 0$. Remember that the hamiltonian is given by

$$H = L_{L,0} + L_{R,0} - c/12. \tag{4.19}$$

It follows that for $c = 1$ the energy of a state is given by $E = h_R + h_L - 1/12$.
Let us now see what the effect of the supercharges is. We write the supercharges as

$$G_L^{\pm} = V_{\pm 1,\pm 3/2} \quad \text{and} \quad G_R^{\pm} = V_{\pm 1,\mp 3/2}. \tag{4.20}$$

As an example we consider the action of the supercharge G_L^+ on a state $V_{m,n}|0\rangle$. Remember that G_L^+ has conformal weight $(h_L, h_R) = (3/2, 0)$. The mode expansion for a purely holomorphic (purely left moving) field ϕ of conformal weight $(h, 0)$ is given by

$$\phi(z) = \sum_l z^{-l-h}\phi_l, \tag{4.21}$$

which is chosen such that ϕ_{-l} has conformal weight l (under $z \to z/\lambda$ we have $\phi(z) \to \lambda^h\phi(z/\lambda)$ from which it follows that $\phi_{-l} \to \lambda^l\phi_{-l}$). The modes satisfy

$$\phi_l = \oint \frac{dz}{2\pi\imath} z^{l+h-1}\phi(z). \tag{4.22}$$

So we find the following mode expansion for G_L^+

$$G_{L,l}^+ = \oint \frac{dz}{2\pi\imath} z^{l+1/2} G_L^+ = \oint \frac{dz}{2\pi\imath} z^{l+1/2} V_{1,3/2}, \tag{4.23}$$

where $l \in \mathbb{Z}$ in the Ramond sector and $l \in (\mathbb{Z} + 1/2)$ in the NS sector. Consequently, we have

$$G_{L,l}^+ V_{m,n}|0\rangle = \oint \frac{dz}{2\pi\imath} z^{l+1/2} V_{1,3/2} V_{m,n}|0\rangle. \tag{4.24}$$

We can also compute the OPE for $G_L^+(z)V_{m,n}(w,\overline{w})$. We use that for a vertex operator $V_\alpha(z) = \exp(\imath\alpha\phi(z))$ of conformal weight $h = \alpha^2/(4g)$ the OPE is given by (see [42])

$$V_\alpha(z)V_\beta(w) \sim (z-w)^{\alpha\beta/(2g)} V_{\alpha+\beta}(w).$$

Using $\alpha_{L,R} = (m \pm 2n/3)$, we find

$$\begin{aligned} G_L^+(z)V_{m,n}(w,\overline{w}) &\sim (z-w)^{(2)(m+2n/3)3/4} \times (\overline{z}-\overline{w})^{(0)(m-2n/3)3/4} \\ &\quad \times \exp(\imath[(1+m)\Phi(w,\overline{w}) + (3/2+n)\tilde{\Phi}(w,\overline{w})]) \\ &= (z-w)^{3/2m+n} V_{m+1,n+3/2}(w,\overline{w}). \end{aligned} \tag{4.25}$$

Finally, combining (4.24) and (4.25) gives

$$G_{L,l}^+ V_{m,n}(0,0)|0\rangle = \oint \frac{dz}{2\pi\imath} z^{3/2m+n+l+1/2} V_{m+1,n+3/2}|0\rangle. \tag{4.26}$$

Similarly, we obtain

$$\begin{aligned} G^-_{L,l} V_{m,n}(0,0)|0\rangle &= \oint \frac{dz}{2\pi\imath} z^{-3/2m-n+l+1/2} V_{m-1,n-3/2}|0\rangle, \\ G^+_{R,l} V_{m,n}(0,0)|0\rangle &= \oint \frac{dz}{2\pi\imath} \overline{z}^{3/2m+n+l+1/2} V_{m+1,n-3/2}|0\rangle, \\ G^-_{R,l} V_{m,n}(0,0)|0\rangle &= \oint \frac{dz}{2\pi\imath} \overline{z}^{-3/2m-n+l+1/2} V_{m-1,n+3/2}|0\rangle. \end{aligned}$$

For the contour integrals to be well-defined the power of z or $\overline{z}$ has to be integer. Since l is integer (half-integer) in the Ramond (NS) sector, we find $3/2m + n$ is half-integer (integer) in the Ramond (NS) sector. This condition can be reformulated by saying that $(-1)^{m+2n}$ is 1 in the Neveu-Schwarz sector and -1 in the Ramond sector.
Furthermore, we see that the first mode $G^+_{L,l}$ of G^+_L that gives a non-zero contribution must obey $3/2m + n + l + 1/2 \leq -1$, i.e. $l \leq -3/2 - 3/2m - n$. Equivalently, we find for $G^-_{L,l}$: $l \leq -3/2 + 3/2m + n$ and for $G^\pm_{R,l}$: $l \leq -3/2 \mp 3/2m \pm n$.
From the above relations it also follows that by acting on a vertex operator with certain combinations of the supercharges we can raise or lower n by multiples of 3 while keeping m fixed. At the same time, the supercharges change m by ± 1, while leaving $(-1)^{m+2n}$ unchanged. From this, it follows that we need only three vertex operators per sector, since all other vertex operators can be generated from these states with the supercharges. For example, one can easily check that $V_{0,-5/2}|0\rangle = G^+_{R,-1} G^-_{L,-1} V_{0,1/2}|0\rangle$ and $V_{-1,-1}|0\rangle = G^-_{L,-1} V_{0,1/2}|0\rangle$.
In the Ramond sector, we choose the highest weight states $V_{0,\pm 1/2}|0\rangle$ and $V_{0,3/2}|0\rangle$, since these are the states with lowest energy. Their conformal dimensions are $h_{L,R} = 1/24$ and $h_{L,R} = 3/8$, respectively, and thus their energies are $E = 0$ and $E = 2/3$. Clearly, the same reasoning applies in the Neveu-Schwarz sector and the highest weight states are $V_{0,0}|0\rangle$ and $V_{0,\pm 1}|0\rangle$ with $h_{L,R} = 0$ and $h_{L,R} = 1/6$ respectively.
We can now compare this to the conformal dimensions of the minimal model in the supersymmetric minimal series given in section 3.4. The free boson has central charge $c = 1$, which corresponds to the first ($k = 1$) minimal model (see (3.14)). The highest weight states of the first minimal model in the supersymmetric minimal series can be found from (3.15) with $k = 1$ and $\alpha = 0, 1/2$ in the Ramond and Neveu-Schwarz sector, respectively:

$$\begin{aligned} h &= \frac{1}{24}, \frac{1}{24}, \frac{3}{8} \qquad \text{(R)} \\ h &= 0, \frac{1}{6}, \frac{1}{6} \qquad \text{(NS)}. \end{aligned}$$

This agrees nicely with the highest weight states we identified above. Finally, remember that the two states with $h = 1/24$ are the zero energy states, corresponding to the Witten index of the first ($k = 1$) minimal model: $W_1 = 2$.
To obtain the corresponding $U(1)$ charges, we consider the OPE of $\partial\Phi$ and a vertex operator V_α with conformal dimension $h = \alpha^2/(4g)$

$$\partial\Phi(z) V_\alpha(w) \sim -\frac{\imath\alpha}{2g} \frac{V_\alpha}{(z-w)}. \tag{4.27}$$

The $U(1)$ current, however, satisfies the following OPE with a primary field ψ

$$J(z)\psi(w) \sim \frac{q}{(z-w)}\psi(w). \tag{4.28}$$

Using (4.18) and the fact that the vertex operators $V_{m,n}$ have $\alpha_{L,R} = (m \pm 2n/3)$, we find

$$\begin{aligned} J_L(z)V_{m,n}(0,0) &\sim (m/2+n/3)\frac{V_{m,n}}{z} \equiv q_L\frac{V_{m,n}}{z}, \\ J_R(\overline{z})V_{m,n}(0,0) &\sim -(m/2-n/3)\frac{V_{m,n}}{\overline{z}} \equiv q_R\frac{V_{m,n}}{\overline{z}}, \end{aligned}$$

where we defined the $U(1)$ charges

$$q_{L,R} = n/3 \pm m/2. \tag{4.29}$$

For the highest weight states in the Ramond and Neveu-Schwarz sector, we readily verify that $q_{L,R}$ are in accordance with the values for the first minimal model (see (3.15))

$$q_{L,R} = \frac{-1/2+\alpha}{3}, \frac{1/2+\alpha}{3}, \frac{3/2+\alpha}{3}. \tag{4.30}$$

Note that α here refers to the sector of the theory ($\alpha = 0$ in the Ramond sector and $\alpha = 1/2$ in the Neveu-Schwarz sector) and should not be confused with $\alpha_{L,R}$ which are related to the conformal dimensions of the vertex operators.
Supersymmetry implies that the zero energy states in the Ramond sector do not have superpartners. Consequently, they must be annihilated by the zero modes of the supercharges, that is $G^{\pm}_{R,L,0}$. From the inequalities relating the mode l to m and n given above, we find that indeed $G^{\pm}_{R,L,0}V_{0,\pm 1/2}|0\rangle = 0$. The third highest weight state in the Ramond sector, $h_{L,R} = 3/8$, has non-zero energy, so we would expect this state to have a superpartner. In fact, since the left and right movers completely decouple in the continuum limit, the continuum theory has two $\mathcal{N} = 2$ supersymmetries. Consequently, the third highest weight state forms a quadruplet instead of a doublet. We find that there are four states with $h_{L,R} = 3/8$ and energy $E = 3/8 + 3/8 - 1/12 = 2/3$, which are all related via the supercharges

$$\begin{aligned} G^{-}_{L,0}V_{0,3/2}|0\rangle &= V_{-1,0}|0\rangle, \\ G^{+}_{R,0}V_{0,3/2}|0\rangle &= V_{1,0}|0\rangle, \\ G^{-}_{L,0}G^{+}_{R,0}V_{0,3/2}|0\rangle &= G^{+}_{R,0}G^{-}_{L,0}V_{0,3/2}|0\rangle = V_{0,-3/2}|0\rangle. \end{aligned}$$

A pictorial summary of the above can be found in figure 4.2.
This concludes this section, since one can now construct all states in the spectrum from the three highest weight states in a given sector using the Virasoro operators and the supercharges.

4.7.2 Lattice operators: fermion number and momentum

In the previous section we discussed the energy spectrum. In the lattice model a state can be characterized, not only by its energy, but also by momentum and fermion number.

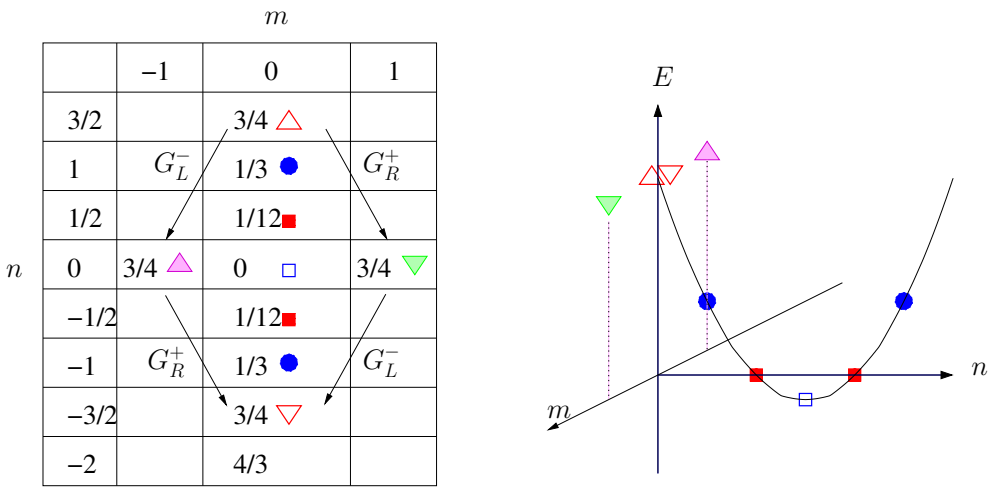

Figure 4.2: The table shows $h_L + h_R = 3/4m^2 + 1/3n^2$, where $(-1)^{m+2n}$ is $+1$ in the NS and -1 in the R sector. The big arrows point at the superpartners of the state with $h_L + h_R = 3/4$. The symbols can be found in the 3D plot, where the energy $E = h_L + h_R - c/12$ is plotted against n and m.

In this section we will identify the corresponding properties in the superconformal field theory.
Remember that the model on the one dimensional periodic chain with length $L = 0$ mod 3 has two $E = 0$ ground states. The ground states have fermion number $f_{GS} = L/3$. In the lattice model each non-zero energy state always has a superpartner with one fermion less or more. Inspection of the action of the supercharges, allows us to identify the index m of a vertex operator $V_{m,n}$ as the charge difference with respect to the ground state charge (or fermion number) in the lattice model: $m = f - f_{GS} = f - L/3$. Using the definition of the $U(1)$ charges (4.29) we can write

$$f - f_{GS} = q_L - q_R = m \tag{4.31}$$

and identify the fermion number operator on the lattice with the difference of the $U(1)$ currents:

$$F = J_{L,0} - J_{R,0} + f_{GS}. \tag{4.32}$$

In the lattice model the translation operator T commutes with both the hamiltonian H and fermion number operator F. The eigenvalues t of the translation operator satisfy $t^L = 1$. In the field theory the operator that generates translations in the space direction corresponds to rotations on the complex plane. The momentum operator on the lattice is thus proportional to $L_{L,0} - L_{R,0}$. All highest weight states in the field theory have $h_L = h_R$, which would thus imply zero momentum. However, we know (see 4.3.2) that the zero-energy states in the Ramond sector do not have zero momentum. In the following we will identify the operator that gives the momenta of the highest weight states.
Let us introduce the boundary condition that the wavefunction picks up a factor $\exp(2\pi\imath\alpha)$ when a fermion hops over the end of the chain, i.e. between site L and site 1. This boundary condition is called a twisted boundary condition. For $\alpha = 0$ we have periodic boundary conditions, which corresponds to the Ramond sector (see 3.5), whereas for

$\alpha = 1/2$ we have anti-periodic boundary conditions, corresponding to the Neveu-Schwarz sector. Consequently, the boundary twist in the lattice model corresponds to a spectral flow in the continuum theory (see section 3.6).
In the following we will show, on the one hand, that the momentum of a state in the lattice model depends linearly on the boundary twist and, on the other hand, that also the index n of a vertex operator $V_{m,n}$ will change linearly under spectral flow. These observations will allow us to relate the two.
Momentum, $p \mod 2\pi$, can be defined by writing the eigenvalues of the translation operator as $t = e^{\imath p}$. The boundary twist can be implemented by replacing the term that hops a particle over the boundary $c_L^\dagger c_1 +$ h.c. by $e^{2\pi\imath\alpha}(c_L^\dagger c_1 +$ h.c.). The eigenvalues of the translation operator for general α then follow from

$$T_\alpha^L|\psi\rangle \;=\; e^{\imath p_0 L} e^{2\pi\imath\alpha f}|\psi\rangle \equiv e^{\imath p_\alpha L}|\psi\rangle, \tag{4.33}$$

where p_0 is the momentum of $|\psi\rangle$ for $\alpha = 0$, L is the length of the system and f is the total number of particles in the state $|\psi\rangle$. It follows that momentum indeed depends linearly on the boundary twist: $p_\alpha = p_0 + 2\pi\alpha f/L \mod 2\pi$. In the ground state sector we have $f = L/3$ and thus $p = p_0 + 2\pi\alpha/3 \mod 2\pi$.
Now let us consider the continuum theory. In the previous section we have seen that $(-1)^{m+2n} = \pm 1$ in the Neveu-Schwarz and Ramond sector respectively. In the ground state sector we have $m = 0$. It follows that n is half-integer in the Ramond sector and integer in the Neveu-Schwarz sector. We can thus identify the spectral flow operator that conserves fermion number m, and takes us from the Ramond sector to the Neveu-Schwarz sector, as the operator $V_{0,1/2}$. More generally, the operator $V_{0,\alpha}$ corresponds to the lattice model operator that introduces the boundary twist α.
If we now combine the fact that $p_\alpha = p_0 + 2\pi\alpha/3 + 2\pi\alpha m/L \mod 2\pi$ for a state in the lattice model and $n = n_0 + \alpha$ for an operator in the field theory, we find that p is proportional to n. By eliminating α and using the known results for the zero energy ground states in the lattice model we obtain

$$p = 2\pi n/3 + 2\pi n m/L + f_{GS}\pi \mod 2\pi. \tag{4.34}$$

For the Ramond vacua $V_{0,\pm 1/2}|0\rangle$ we can easily check this relation. We know that the two ground states of the periodic chain of length $L = 3j$ have momenta $p_0 = \pm\pi/3 + \pi f_{GS} \mod 2\pi$. Since the Ramond vacua have $n = \pm 1/2$ and $m = 0$, we find that this indeed nicely agrees with the equation above. Note that the middle term is precisely $2\pi(h_R - h_L)/L$. Finally, using the definition of the $U(1)$ charges (4.29) we can write momentum as

$$p = (q_L + q_R)\pi + 2\pi(h_R - h_L)/L + f_{GS}\pi \mod 2\pi \tag{4.35}$$

and we find that the momentum operator on the lattice can be expressed as

$$P \;=\; (J_{L,0} + J_{R,0})\pi + (L_{L,0} - L_{R,0})2\pi/L + f_{GS}\pi \mod 2\pi. \tag{4.36}$$

4.7.3 Highest weight state and descendants

We are now fully equipped to construct the entire energy spectrum of the superconformal field theory. We start from the highest weight states and build the spectrum by acting

Table 4.2: In this table we show the descendants of the highest weight state $V_{0,1/2}|0\rangle$. This is one of the two zero energy states in the Ramond sector. We order the descendants by their energy, also called level, in the first column. The energy is given by $E = h_L + h_R - 1/12$. In the second column we give the state $L_{L,-l_1} \dots L_{L,-l_s} L_{R,-r_1} \dots L_{R,-r_q} V_{n,m}|0\rangle_{NS} \equiv |h_L - 1/24 + \sum_{i=1}^{s} l_i, h_R - 1/24 + \sum_{i=1}^{q} r_i\rangle$. In the third column we give $h_L - h_R$, which is directly related to the change in momentum with respect to the highest weight state. In the fourth column we give all the fields that correspond to the state given in the second column and finally, in the last column we give the charge m. The charge gives the change in fermion number with respect to the highest weight state.

Energy	State	$h_L - h_R$	Fields	Charge
0	$\|0,0>$	0	$V_{0,1/2}$	0
1	$\|1,0>$	1	$L_{L,-1}V_{0,1/2}$	0
			$G^-_{L,-1}V_{0,1/2} = V_{-1,-1}$	-1
	$\|0,1>$	-1	$L_{R,-1}V_{0,1/2}$	0
			$G^+_{R,-1}V_{0,1/2} = V_{1,-1}$	1
2	$\|2,0>$	2	$L_{L,-1}L_{L,-1}V_{0,1/2}$	0
			$L_{L,-2}V_{0,1/2}$	0
			$G^+_{L,-2}V_{0,1/2} = V_{1,2}$	1
			$L_{L,-1}G^-_{L,-1}V_{0,1/2} = L_{L,-1}V_{-1,-1}$	-1
	$\|1,1>$	0	$L_{L,-1}L_{R,-1}V_{0,1/2}$	0
			$L_{R,-1}G^-_{L,-1}V_{0,1/2} = L_{R,-1}V_{-1,-1}$	-1
			$L_{L,-1}G^+_{R,-1}V_{0,1/2} = L_{L,-1}V_{1,-1}$	1
			$G^+_{R,-1}G^-_{L,-1}V_{0,1/2} = V_{0,-5/2}$	0
	$\|0,2>$	-2	$L_{R,-1}L_{R,-1}V_{0,1/2}$	0
			$L_{R,-2}V_{0,1/2}$	0
			$G^-_{R,-2}V_{0,1/2} = V_{-1,2}$	-1
			$L_{R,-1}G^+_{R,-1}V_{0,1/2} = L_{R,-1}V_{1,-1}$	1
...				

on these states with the operators $L_{(R,L),-n}$ and $G^{\pm}_{(R,L),-l}$, with $l, n > 0$. Let us work out an example. We start from one of the Ramond vacua: $V_{0,1/2}|0\rangle$. It is now convenient to write a highest weight state as $V_{n,m}|0\rangle_{NS} = |h_L - 1/24, h_R - 1/24\rangle$, so for the Ramond vacuum under consideration we write $V_{0,1/2}|0\rangle = |0,0\rangle$. The action of $L_{L,-n}$ is now simply $L_{L,-n}|h_L - 1/24, h_R - 1/24\rangle = |h_L - 1/24 + n, h_R - 1/24\rangle$ and similarly for $L_{R,-n}$. Putting everything together, we summarize the spectrum that follows from this particular highest weight state in table 4.2 and in figure 4.3. The energy follows from $E = h_L + h_R - 1/12$, momentum is given by $P = 2\pi(h_L - h_R)/L + p$, with $p = 2\pi n/3 + f\pi \mod 2\pi$ and the charge is simply m. Since p is left unchanged by both the Virasoro operators as well as the supercharges, all states generated from the Ramond vacuum $V_{0,1/2}|0\rangle$ have momentum $P = 2\pi(h_L - h_R)/L + \pi/3 + f_{GS}\pi \mod 2\pi$. To save space, we just give $h_L - h_R$ in the table.

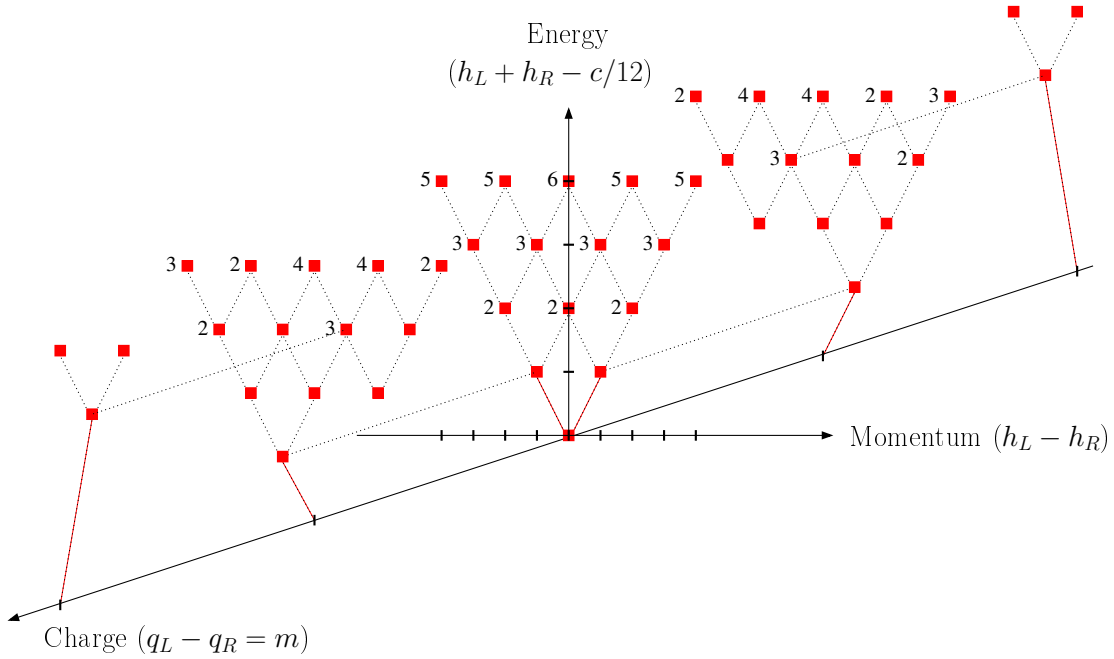

Figure 4.3: We depict the highest weight state $V_{0,1/2}|0\rangle$ and its descendants in a 3D plot. The energy (first column in table 4.2) runs on the vertical axis. Horizontally, we plot the momentum $h_L - h_R$ and the fermion number m relative to the highest weight state (third and last column in table 4.2). The labels indicate the degeneracy of the state (states with no label are non-degenerate). Finally, the dotted lines serve as guides to the eye.

4.7.4 Partition sum

In this section we briefly discuss the partition sum and character formula's. Remember that computing the partition sum at finite temperature is equivalent to computing the path integral with the imaginary time direction compactified. Let w be the complex coordinate parametrizing the cylinder, where time runs along the cylinder. We know that translations in the time direction are generated by the hamiltonian, whereas translations in the space direction are generated by the momentum operator. To compactify the time direction we need to identify two periods in w defining a torus: $w \equiv w + 2\pi\omega_1$ and $w \equiv w + 2\pi\omega_2$. Because of conformal invariance this can be rescaled, so that there is only one parameter characterizing the torus, the modular parameter, $\tau = \omega_2/\omega_1$. Clearly, the modular parameter is a complex parameter and can be written as $\tau = \tau_1 + \imath\tau_2$, with τ_1 and τ_2 real parameters. It now follows that a translation in space-time along the τ direction over a distance a is given by the operator

$$\exp\left[-\frac{a}{2\pi|\tau|}(2\pi H\tau_2 - 2\pi\imath P\tau_1)\right]. \tag{4.37}$$

If we now consider a as the lattice spacing in a two dimensional statistical mechanical model, the above parameter is simply the transfer matrix from one row in the model to the next. It follows that we can write the partition sum as the trace over this operator to the power l (see also section 4.3.1), such that $al = 2\pi|\tau|$, the period of the system. So we find

$$Z = \mathrm{Tr}\ \exp\left[-2\pi H\tau_2 + 2\pi\imath P\tau_1\right]. \tag{4.38}$$

Using the expressions of H and P on the cylinder in terms of the Virasoro generators, we find

$$\begin{aligned} Z &= \text{Tr } \exp\left[-2\pi(L_0 - c/24 + \overline{L}_0 - \overline{c}/24)\tau_2 + 2\pi\imath(L_0 - c/24 - \overline{L}_0 + \overline{c}/24)\tau_1\right] \\ &= \text{Tr } \exp\left[2\pi\imath\tau(L_0 - c/24)\right] \exp\left[-2\pi\imath\overline{\tau}(\overline{L}_0 - \overline{c}/24)\right] \\ &= \text{Tr } q^{L_0 - c/24}\overline{q}^{\overline{L}_0 - \overline{c}/24}, \end{aligned} \tag{4.39}$$

where $q \equiv e^{2\pi\imath\tau}$.
To find an explicit expression for the partition sum, we thus have to compute the traces of $q^{L_0-c/24}$ and $\overline{q}^{\overline{L}_0-\overline{c}/24}$. Since the spectrum decomposes in highest weight states and their descendants, it is convenient to also decompose the trace this way. A highest weight state of conformal dimension h has $L_0|h\rangle = h|h\rangle$ and its descendants have $L_0 L_{-n_k} \dots L_{-n_2} L_{-n_1}|h\rangle = (h + n_k + \dots + n_2 + n_1) L_{-n_k} \dots L_{-n_2} L_{-n_1}|h\rangle$, with all n_i positive. The trace of $q^{L_0-c/24}$ restricted to this highest weight state and its descendants is called the character, usually denoted by $\chi_h(q)$. We find that

$$\chi_h(q) = \sum_n \dim(h+n) q^{h+n-c/24}, \tag{4.40}$$

where $\dim(h+n)$ denotes the number of linearly independent states at level n. It can be shown that this number is precisely $p(n)$, the number of integer partitions of n. Since the generating function of $p(n)$ is given by

$$\sum_n p(n) x^n = \prod_{k=1}^{\infty} (1 - x^k)^{-1}, \tag{4.41}$$

we find

$$\begin{aligned} \chi_h(q) &= \sum_n p(n) q^{h+n-c/24} \\ &= q^{h-c/24} \prod_{k=1}^{\infty} (1 - q^k)^{-1}. \end{aligned} \tag{4.42}$$

In the literature one usually defines $\eta(q) \equiv q^{c/24} \prod_{k=1}^{\infty}(1-q^k)$, such that the character can be written as $\chi_h(q) = q^h/\eta(q)$.
Remembering that for the free boson we have $c = \overline{c} = 1$ and conformal dimensions $h_{L,R}(m,n) = (m \pm gn)^2/(4g)$, we can write the partition sum as

$$\begin{aligned} Z &= \text{Tr } q^{L_0 - 1/24}\overline{q}^{\overline{L}_0 - 1/24} \\ &= \frac{1}{\eta\overline{\eta}} \sum_{m,n} q^{h_L(m,n)} \overline{q}^{h_R(m,n)} \\ &= \frac{1}{\eta\overline{\eta}} \sum_{m,n} q^{(m+gn)^2/(4g)} \overline{q}^{(m-gn)^2/(4g)}, \end{aligned} \tag{4.43}$$

with $\overline{\eta} = \eta(\overline{q})$ and $\eta(q) = q^{1/24} \prod_{k=1}^{\infty}(1-q^k)$. Finally, the coupling g is related to the compactification radius as $g = 2/R^2$.

4.7.5 Fermi velocity

The finite-size scaling of the energy depends on the boundary conditions. For (anti-) periodic boundary conditions, which corresponds to the cylinder on the field theory side, the scaling is given by [63, 64]

$$E_{\text{num}} = 2\pi E_{\text{SCFT}} v_F / N + \mathcal{O}(1/N^2), \tag{4.44}$$

where N is the length of the finite system and v_F the Fermi velocity. It follows that by comparing the finite size spectra with the spectrum of the field theory one can extract the Fermi velocity. In this case, however we can also obtain the Fermi velocity using the mapping of the supersymmetric model onto the XXZ chain. For the XXZ chain (4.11) the Fermi velocity is given by

$$v_F(\Delta) = \pi \sin\theta/\theta, \tag{4.45}$$

with $\cos\theta = -\Delta$. The supersymmetric model maps to the XXZ chain with $\Delta = -1/2$, so we find $\theta = \pi/3$ and the Fermi velocity of the corresponding XXZ chain is $v_F = (3\sqrt{3})/2$. To find the Fermi velocity for the supersymmetric model, we note that the length N of XXZ chain is related to the length L of the supersymmetric chain via $N = L - f$, where f is the number of fermions in the supersymmetric model [23]. In the continuum limit the low energy states have approximately $f = L/3$, so $N = 2L/3$. Combining all this, we find for the supersymmetric model that

$$E_{\text{num}} = 2\pi E_{\text{SCFT}} v_F / L + \mathcal{O}(1/L^2), \tag{4.46}$$

with Fermi velocity $v_F = 3/2 v_{F,XXZ} = (9\sqrt{3})/4$.

4.7.6 Chain of length $L = \pm 1 \mod 3$

In the previous sections we have identified the Ramond sector of the field theory to correspond to the lattice model on a chain with length $L = 0 \mod 3$ with periodic boundary conditions. For the chain of length $L = 3j$, the fermion number in the ground state sector is $f_{GS} = L/3 = j$. For a chain of length $L = 3j \pm 1$, we would correspondingly find $f_{GS} = L/3 = j \pm 1/3$. We know, however, that for a chain of length $L = 3j \pm 1$ the ground state has fermion number $f_{GS} = j$. It follows that, compared to the chain of length $L = 3j$, the chain of length $L = 3j \pm 1$ has a slightly lower/higher charge density in the ground state sector. Now remember that m gives the charge compared to the charge in the ground state sector of the chain of length $L = 3j$, that is $L/3$. Suppose that instead of $m = f - f_{GS}$, we now write $m = f - L/3$. For the chain of length $L = 3j$, the two definition are completely equivalent. However, for a chain of length $L = 3j \pm 1$ we now find that $m = f_{GS} - L/3 = \mp 1/3$ in the ground state sector. The supersymmetry in the lattice model tells us that the chain with periodic boundary conditions corresponds to the Ramond sector in the field theory. Now that m takes values in $\mathbb{Z} \mp 1/3$, it follows that in the Ramond sector, which has $3m/2 + n \in \mathbb{Z} + 1/2$, n is now integer. In fact, we find that adding or subtracting one site from a chain of length $L = 3j$ corresponds in the field theory to acting with the operator $V_{\mp 1/3,-1/2}$. Upon acting with this operator the highest weight states in the Ramond sector become

$$V_{\mp 1/3,-1}|0\rangle, V_{\mp 1/3,0}|0\rangle \text{ and } V_{\mp 1/3,1}|0\rangle, \tag{4.47}$$

for the chains of length $L = 3j \pm 1$. The corresponding energies are respectively $E = 1/3, 0$ and $1/3$. This agrees with the fact that these chain lengths only have one zero energy ground state. Furthermore, we see that, since the ground state has $n = 0$, it has the correct momentum $p = 0 + j\pi \mod 2\pi$.

4.7.7 Finite size spectra

In this section we analyze the numerically obtained spectra for the supersymmetric model on the chain with periodic and anti-periodic boundary conditions. We consider lengths up to $L = 27$. Since the hamiltonian commutes with the fermion number operator F and translation operator T, we can block diagonalize the hamiltonian. To do this we construct a basis of eigenstates of F and T. The first is straightforward since each configuration is an eigenstate of F, since it has a well defined particle number. The latter requires a bit more work. An eigenstate of T clearly obeys

$$T|\Psi\rangle = t|\Psi\rangle. \tag{4.48}$$

Given a certain configuration $|C\rangle$, we can construct an eigenstate of T by writing

$$|\Psi\rangle = \sum_{l=1}^{L} t^{-l}(T)^l|C\rangle. \tag{4.49}$$

The slightly subtle part now concerns the possible values of t. Remember that for a state with f fermions the eigenvalues of T satisfy $t^L = e^{2\pi\imath\alpha f}$, with $\alpha = 0$ for periodic bc and $\alpha = 1$ for anti-periodic bc. It follows that in principle t can take all values $t_k = e^{2\pi\imath(\alpha f+k)/L}$, with $k = 1, 2, \ldots, L$. This is not true, however, if the configuration $|C\rangle$ maps onto itself under the action of T^n, with $n < L$, that is

$$T^n|C\rangle = (-1)^s e^{2\pi\imath\alpha f n/L}|C\rangle, \tag{4.50}$$

with $s = f^2 n(L-n)/L^2$, is the sign that comes from the Fermi statistics of the particles (nf/L fermions hop over $(L-n)f/L$ fermions). It then follows that t can only take the values $t_k = e^{2\pi\imath(\alpha f/L + s/2n + k/n)}$, with $k = 1, 2, \ldots, n$.
Upon using these symmetries the hamiltonian block diagonalizes into blocks $H_{f,t}$. At length $L = 27$ the largest block has $f = 8$ and $t = e^{2\pi\imath(\alpha 8+k)/27}$, with $k = 1, \ldots, 27$. The dimension of the Hilbert space in this sector is 4000. This matrix size can be effectively handled by the built-in diagonalization scheme of Matlab.
We have concluded in the previous sections that chains of length $L = 3j$ with anti-periodic bc correspond to the vacuum sector of the superconformal field theory. Indeed numerically, we find that for these systems there is one negative energy state with fermion number $f = L/3$ (see figure 4.4(f) for an example). In figure 4.5(a) the energy of this state is plotted for various system sizes as a function of one over the length of the system. Remember that the scaling is given by [63, 64]

$$E_{\text{num}} = 2\pi E_{\text{SCFT}} v_F/L + \mathcal{O}(1/L^2), \tag{4.51}$$

where $E_{\text{SCFT}} = h_L + h_R - c/12$ and $v_F = 9\sqrt{3}/4$. For the vacuum we have $h_L = h_R = 0$ and since $c = 1$, we find that the energy of these states scales as $E_{\text{num}} = -3\sqrt{3}\pi/(8N) \approx$

$-2.041/N$. The function that gives the best fit to the numerics is $f(L) = a/L+b/L^2+c/L^3$ with $a = -2.038$, $b = -0.056$ and $c = -6.509$. Clearly, the value of a agrees well with the theoretical value.

We perform this scaling analysis for all highest weight states and some descendants for all boundary conditions, that is periodic and anti-periodic and lengths $L = 3j$ and $L = 3j \pm 1$. In the field theory these boundary condition correspond to the Ramond and Neveu-Schwarz sectors and the untwisted ($L = 3j$) and twisted ($L = 3j \pm 1$) sectors. By twisted sectors, we mean the sectors where m takes values in $\mathbb{Z} \pm 1/3$ (see section 4.7.6). We have plotted the spectra of the largest system sizes for the particle numbers at which the highest weight states occur and indicated for which states we performed the scaling analysis (fig. 4.4). The scaling data and the fits are shown in figure 4.5. The results are summarized in table 4.3.

An interesting point is that for the periodic chain of length $L = 3j$, the two states that correspond to the fields $V_{0,\pm 3/2}$ are not degenerate at finite size (in figure 4.4(e)) these are the states with labels 3 and 4). The same is true for the states with labels 5 and 6 in 4.4(e) which correspond to the fields $L_{-1;L/R}V_{0,1/2}$. Since the model is exactly solvable, we know that this must be a finite size effect and should thus vanish in the continuum limit (see also [65]). For the two states that correspond to the fields $V_{0,\pm 3/2}$, we checked this explicitly by verifying that the energy difference between the two states goes to zero faster than one over the length of the system. Indeed, we find that the energy difference scales as $a/L^2 + b/L^3$, with $a = 52$ and $b = -86$.

Remarkably, we find that the states with the higher energy have superpartners at $f = j+1$, whereas the states with lower energy have superpartners at $f = j - 1$. This is probably explained as follows. The continuum limit holds for systems of infinite size close to or at 1/3 filling. In the continuum limit there is a particle-hole symmetry corresponding to the mapping $m, n \to -m, -n$. In a finite size system, however, the particle-hole symmetry is not realized, because of the nearest-neighbor exclusion rule. At 1/3 filling it thus costs more energy to add a particle than to take out a particle, since one is closer to the completely full system than the completely empty system.

Another way to see this is via the mapping to the XXZ chain. The supersymmetric model on a chain of length L at 1/3 filling corresponds to the XXZ chain of length N at zero magnetization. The two chain lengths are related via $N = L - f$, where f is the number of fermions in the supersymmetric model. It follows that the supercharges which add or remove a fermion in the supersymmetric model translate into operators on the spin chain which change the length of the chain. Since the energy scales as one over the length, a states with more particles in the supersymmetric model, which has a shorter length in the XXZ chain, will thus have a higher energy. Conversely, a state with less particles will have a lower energy.

4.8 Spectral flow

In superconformal field theory one can define a spectral flow operator that maps the Ramond sector to a sector with $r \in \mathbb{Z}+\alpha$, where r labels the modes in the mode expansion of the supercharge (3.6). In this section we will discuss the effect of this operator on the states, first for a general superconformal field theory (see also section 3.6) and later for the first supersymmetric minimal model in particular. In the lattice model the spectral

Table 4.3: This table contains a summary of the data extracted from the finite size spectra and the scaling fits. The first column contains the labels which can be found in figures 4.4 and 4.5. In the last column, we defined $P'_{\text{num}} \equiv P_{\text{num}} + \pi j \mod 2\pi$.

$L = 3j$

label	BC	n	field	E_{SCFT}	$h_L - h_R$	$(q_L + q_R)\pi$	$E_{\text{num}}L/(2\pi v_F)$	P'_{num}
1	R	$-\frac{1}{2}$	$V_{0,-\frac{1}{2}}$	0	0	$\frac{5\pi}{3}$	0	$\frac{5\pi}{3}$
2	R	$\frac{1}{2}$	$V_{0,\frac{1}{2}}$	0	0	$\frac{\pi}{3}$	0	$\frac{\pi}{3}$
3	R	$-\frac{3}{2}$	$V_{0,-\frac{3}{2}}$	$\frac{2}{3}$	0	π	0.670	π
4	R	$\frac{3}{2}$	$V_{0,\frac{3}{2}}$	$\frac{2}{3}$	0	π	0.666	π
5	R	$\frac{1}{2}$	$L_{L,-1}V_{0,\frac{1}{2}}$	1	1	$\frac{\pi}{3}$	1.004	$\frac{\pi}{3} + \frac{2\pi}{L}$
6	R	$\frac{1}{2}$	$L_{R,-1}V_{0,\frac{1}{2}}$	1	-1	$\frac{\pi}{3}$	0.997	$\frac{\pi}{3} - \frac{2\pi}{L}$
7	NS	0	$V_{0,0}$	$-\frac{1}{12}$	0	0	-0.0832	0
8	NS	1	$V_{0,1}$	$\frac{1}{4}$	0	$\frac{2\pi}{3}$	0.250	$\frac{2\pi}{3}$
9	NS	-1	$V_{0,-1}$	$\frac{1}{4}$	0	$\frac{4\pi}{3}$	0.250	$\frac{4\pi}{3}$

$L = 3j + 1$

label	BC	n	field	E_{SCFT}	$h_L - h_R$	$(q_L + q_R)\pi$	$E_{\text{num}}L/(2\pi v_F)$	P'_{num}
1	R	0	$V_{-\frac{1}{3},0}$	0	0	0	0	0
2	R	-1	$V_{-\frac{1}{3},-1}$	$\frac{1}{3}$	0	$\frac{4\pi}{3}$	0.333	$\frac{4\pi}{3} + \frac{2\pi}{9j}$
3	R	1	$V_{-\frac{1}{3},1}$	$\frac{1}{3}$	0	$\frac{2\pi}{3}$	0.333	$\frac{2\pi}{3} - \frac{2\pi}{9j}$
4	R	0	$L_{L,-1}V_{-\frac{1}{3},0}$	1	1	0	1.001	$\frac{2\pi}{L}$
5	R	0	$L_{R,-1}V_{-\frac{1}{3},0}$	1	-1	0	1.001	$-\frac{2\pi}{L}$
6	NS	$\frac{1}{2}$	$V_{-\frac{1}{3},\frac{1}{2}}$	$\frac{1}{12}$	0	$\frac{\pi}{3}$	0.0831	$\frac{\pi}{3} - \frac{\pi}{9j}$
7	NS	$-\frac{1}{2}$	$V_{-\frac{1}{3},-\frac{1}{2}}$	$\frac{1}{12}$	0	$\frac{5\pi}{3}$	0.0831	$\frac{5\pi}{3} + \frac{\pi}{9j}$
8	NS	$\frac{3}{2}$	$V_{-\frac{1}{3},\frac{\pm 3}{2}}$	$\frac{3}{4}$	0	π	0.752	$\pi \pm \frac{\pi}{3j}$

$L = 3j - 1$

label	BC	n	field	E_{SCFT}	$h_L - h_R$	$(q_L + q_R)\pi$	$E_{\text{num}}L/(2\pi v_F)$	P'_{num}
1	R	0	$V_{\frac{1}{3},0}$	0	0	0	0	0
2	R	-1	$V_{\frac{1}{3},-1}$	$\frac{1}{3}$	0	$\frac{4\pi}{3}$	0.333	$\frac{4\pi}{3} - \frac{2\pi}{9j}$
3	R	1	$V_{\frac{1}{3},1}$	$\frac{1}{3}$	0	$\frac{2\pi}{3}$	0.333	$\frac{2\pi}{3} + \frac{2\pi}{9j}$
4	R	0	$L_{L,-1}V_{\frac{1}{3},0}$	1	1	0	1.002	$\frac{2\pi}{L}$
5	R	0	$L_{R,-1}V_{\frac{1}{3},0}$	1	-1	0	1.002	$-\frac{2\pi}{L}$
6	NS	$\frac{1}{2}$	$V_{\frac{1}{3},\frac{1}{2}}$	$\frac{1}{12}$	0	$\frac{\pi}{3}$	0.0835	$\frac{\pi}{3} + \frac{\pi}{9j}$
7	NS	$-\frac{1}{2}$	$V_{\frac{1}{3},-\frac{1}{2}}$	$\frac{1}{12}$	0	$\frac{5\pi}{3}$	0.0835	$\frac{5\pi}{3} - \frac{\pi}{9j}$
8	NS	$\frac{3}{2}$	$V_{\frac{1}{3},\frac{\pm 3}{2}}$	$\frac{3}{4}$	0	π	0.753	$\pi \pm \frac{\pi}{3j}$

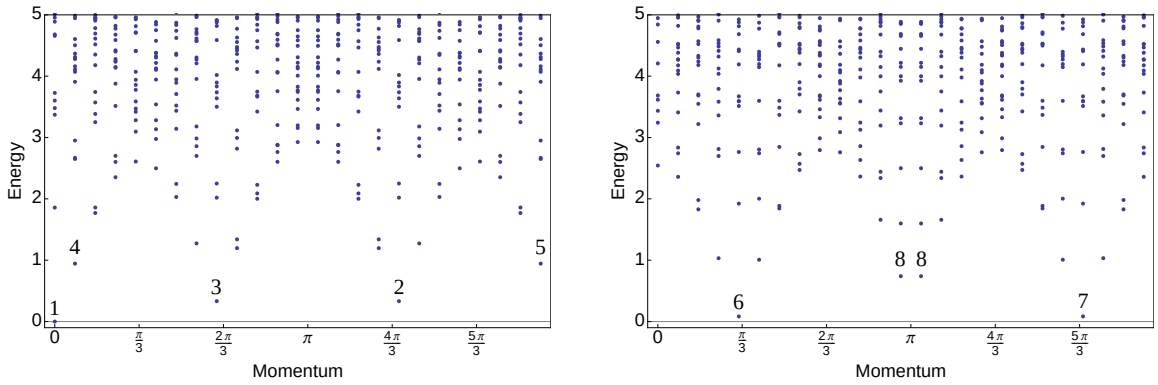

(a) $L = 25,\ f = 8,\ \alpha = 0$ (b) $L = 25,\ f = 8,\ \alpha = 1/2$

(c) $L = 26,\ f = 9,\ \alpha = 0$ (d) $L = 26,\ f = 9,\ \alpha = 1/2$

(e) $L = 27,\ f = 9,\ \alpha = 0$ (f) $L = 27,\ f = 9,\ \alpha = 1/2$

Figure 4.4: Energy versus momentum for chains of lengths $L = 25, 26, 27$ with periodic ($\alpha = 0$) and anti-periodic ($\alpha = 1/2$) boundary conditions and fermion number $f = \text{int}(L/3)$. The labels of the states refer to the numbers in the first column in table 4.3.

flow operator corresponds to the boundary twist operator. This correspondence will prove very powerful in identifying critical modes in supersymmetric models on ladders. Since the supersymmetric model on the chain is exactly solvable, we know that the spectral flow should correctly describe the boundary twist. We have already seen that the scaling behavior of the finite size spectra nicely corresponds to the behavior one expects from the field theory. However, for more complicated systems extracting the scaling behavior can be very challenging, whereas boundary twists are easily carried out. For this reason we

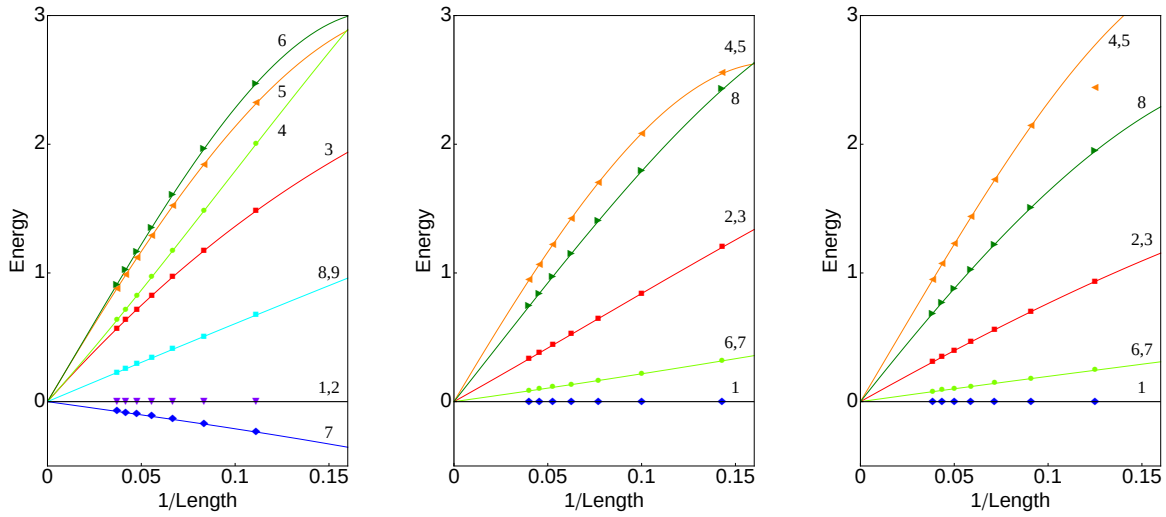

(a) $L = 3j$ (b) $L = 3j + 1$ (c) $L = 3j - 1$

Figure 4.5: Energy versus the inverse chain length for chains with periodic and anti-periodic boundary conditions. The numerical data and fits are shown. The fit function is $f(L) = a/L + b/L^2 + c/L^3$. The labels of the fits refer to the numbers in the first column in table 4.3.

will discuss the spectral flow and boundary twist for the chain here in quite some detail. In general we have that a spectral flow characterized by the parameter α in a superconformal field theory with central charge c has the following effect on the conformal dimensions and charges [49]

$$\begin{aligned} h^{\alpha}_{L,R} &= h^{0}_{L,R} + \alpha q^{0}_{L,R} + \frac{c}{6}\alpha^2 \\ q^{\alpha}_{L,R} &= q^{0}_{L,R} + \frac{c}{3}\alpha. \end{aligned} \tag{4.52}$$

It follows that energy changes parabolically with α under spectral flow

$$E_{\alpha} = E_0 + \alpha(q_L + q_R) + \frac{c}{3}\alpha^2. \tag{4.53}$$

If we define $Q = q_L - q_R$ and $\tilde{Q} = q_L + q_R$, which are related to charge and momentum respectively, we find that under spectral flow

$$\begin{aligned} Q_{\alpha} &= Q_0, \\ \tilde{Q}_{\alpha} &= \tilde{Q}_0 + \frac{2c}{3}\alpha, \end{aligned} \tag{4.54}$$

that is Q is invariant and $\tilde{Q}$ changes linearly with α under spectral flow.
In the lattice model we can go from periodic to anti-periodic boundary conditions continuously by replacing the term that hops a particle over the boundary $c^{\dagger}_{L}c_1 +$ h.c. by $e^{2\pi\imath\alpha}c^{\dagger}_{L}c_1 +$ h.c. The eigenvalues of the translation operator p_{α} will then depend linearly on the twist parameter:

$$T^{L}_{\alpha}|\psi\rangle = e^{\imath p_0 L}e^{2\pi\imath\alpha f}|\psi\rangle \equiv e^{\imath p_{\alpha} L}|\psi\rangle, \tag{4.55}$$

so $p_\alpha = p_0 + 2\pi\alpha f/L \mod 2\pi$ where L is the length of the system and f is the total number of particles in the state $|\psi\rangle$.
To compare the numerical values we obtain for the energy of finite size systems of length L with a boundary twist we use $E_{\text{num}}(\alpha) = 2\pi E_\alpha v_F/L$, where v_F is the Fermi velocity. Using the linear relation between momentum in the lattice model and the twist α, we can express the energy as a parabolic function of momentum

$$E_{\text{num}}(p_\alpha) = 2\pi E_0 v_F/L + \frac{(p_\alpha - p_0)\tilde{Q}_0 v_F}{f} + \frac{c(p_\alpha - p_0)^2 v_F L}{6\pi f^2}$$

It follows that in a finite size system we should be able to fit the energies to the following curve

$$E_{\text{num}}(p_\alpha) = a + bp_\alpha + dp_\alpha^2, \tag{4.56}$$

where the fit parameters b and d will satisfy

$$\begin{aligned} b &= \frac{\tilde{Q}_0 v_F}{f} - \frac{cp_0 L v_F}{3\pi f^2}, \\ d &= \frac{cLv_F}{6\pi f^2}. \end{aligned} \tag{4.57}$$

If we combine this with $E_{\text{num}}(p_{\alpha=0}) = 2\pi E_0 v_F/L$, we have three equations for four parameters in the continuum theory: the central charge c, the energy in the Ramond sector E_0, the sum of the $U(1)$ charges $\tilde{Q}$ and finally the Fermi velocity v_F. It follows that from the energy dependence on a boundary twist, one can extract c, E_0 and $\tilde{Q}$ as functions of the Fermi velocity.
Let us now go back to the supersymmetric model on the chain and thus the first supersymmetric minimal model. In section 4.7.2, we identified the operator $V_{0,\alpha}$ as the operator that corresponds to the boundary twist in the lattice model. Upon comparison with the general expression for the spectral flow operator (3.24) we find that this boundary twist operator is indeed the spectral flow operator:

$$\begin{aligned} U(z,\bar{z}) &= \exp\left[\imath\sqrt{\frac{2gc}{3}}\alpha(\Phi_L - \Phi_R)\right] \\ &= \exp\left[\imath\alpha\tilde{\Phi}\right] \\ &= V_{0,\alpha}. \end{aligned} \tag{4.58}$$

We can easily derive expressions for the energy, momentum and fermion number of the highest weight states under the action of this operator. The operator $V_{0,\alpha}$ leaves m unchanged and sends n to $n+\alpha$, so we find

$$\begin{aligned} f_\alpha &= f_0, \\ E_\alpha &= E_0 + \frac{2n\alpha + \alpha^2}{3}, \\ p_\alpha &= p_0 + \frac{2\pi\alpha}{3} \mod 2\pi. \end{aligned}$$

where f_0, E_0 and p_0 are the values of fermion number, energy and momentum of the highest weight states in the Ramond sector. To check that this agrees with the general spectral flow equations given in (4.53) and (4.54), remember that f and p can be expressed in terms of Q and $\tilde{Q}$ as $f = Q + f_{GS}$ and $p = (\tilde{Q} + f)\pi \mod 2\pi$.

4.8.1 Spectral flow in finite size spectra

In this section we present the data for periodic chains of lengths up to $L = 27$ with a boundary twist. In the lattice model the boundary twist is implemented by replacing the term in the hamiltonian that hops a particle over the boundary $c_L^\dagger c_1 +$ h.c. by $e^{2\pi\imath\alpha}(c_L^\dagger c_1 +$ h.c.). We compute the spectra for various values of α to extract the behavior of the energy as a function of the twist parameter α. Note that the spectrum of the system with twist parameter $-\alpha$ can be obtained from the spectrum with $+\alpha$ using symmetry arguments. To see this we first note that the hamiltonian commutes with T. The eigenvalues of T are $t_k(\alpha) = \exp(2\pi\imath(k+\alpha f)/L)$ with $k = 1, \ldots, L$. Furthermore, the hamiltonian is Hermitian. Since we have $(t_k(\alpha))^\dagger = t_{-k}(-\alpha)$, we find that $E_k(\alpha) = E_{-k}(-\alpha)$, where $E_k(\alpha)$ denotes the energy of a state with momentum $p_k(\alpha) = 2\pi(k + \alpha f)/L \mod 2\pi$. For $2\alpha \in \mathbb{Z}$, we find that $p_k(\alpha) = 2\pi(k + \alpha f)/L \mod 2\pi = \pi k'/L$ and $p_{-k}(-\alpha) = -2\pi(k + \alpha f)/L \mod 2\pi = \pi(2L - k')/L$, with k' between 0 and $2L$. It follows that the spectrum is symmetric around $p = \pi$. However, for $2\alpha \notin \mathbb{Z}$ we find that the spectrum at momentum $p_k(\alpha) = 2\pi(k + \alpha f)/L \mod 2\pi$ for a system with twist parameter α is equal to the spectrum at momentum $p_{-k}(-\alpha) = -2\pi(k + \alpha f)/L \mod 2\pi$ for a system with twist parameter $-\alpha$.

We compute the spectrum of the system for $\alpha = \frac{s}{8}$, with $s = 0, \ldots, 4$. For $s = 0$ ($s = 4$) we have periodic (anti-periodic) boundary conditions. An example is shown in figure 4.6, for the chain of length $L = 27$ and particle number $f = 9$. For the low lying states one can easily see how the energy changes under the boundary twist. The drawn lines are parabolic fits to the energies E_{num} as a function of the momenta p_α. For the two lowest lying states, with $E_{\text{num}} = 0$ for $p_{\alpha=0} = 2\pi/3$ and $p_{\alpha=0} = 4\pi/3$ we find the fits $f(x) = a + bx + dx^2$, with $(a, b, d) = (0.607, -0.435, 0.069)$ and $(a, b, d) = (0.579, -0.422, 0.068)$ respectively. Using equations (4.57) and the usual finite size scaling for the energy, we find

$$\frac{E_\alpha}{c} = \frac{E_{\text{num}}(p_\alpha)L^2}{d12\pi^2 f^2} \tag{4.59}$$

$$\frac{\tilde{Q}_\alpha}{c} = \frac{b + 2dp_\alpha L}{d6\pi f}. \tag{4.60}$$

For the first fit we find $(E_0/c, \tilde{Q}_0/c) = (0, -0.334)$ and $(E_{1/2}/c, \tilde{Q}_{1/2}/c) = (-0.083, 0.000)$ and for the second fit we find $(E_0/c, \tilde{Q}_0/c) = (0, 0.334)$ and $(E_{1/2}/c, \tilde{Q}_{1/2}/c) = (0.254, 0.675)$. It is clear that both fits correspond quite accurately with the theoretically predicted values of $(E_0/c, \tilde{Q}_0/c) = (0, \pm 1/3)$ in the Ramond sector and $(E_{1/2}/c, \tilde{Q}_{1/2}/c) = (-1/12, 0)$ and $(E_{1/2}/c, \tilde{Q}_{1/2}/c) = (1/4, 2/3)$ in the Neveu-Schwarz sector.

Note that the two fits are almost the same, as they should since the fields $V_{0,-1/2}$ and $V_{0,1/2}$ flow into each other under spectral flow, so their energies lie on the same parabola.

In table 4.4 we summarize the values we extract from the parabola fits for $(E_{1/2}/c, \tilde{Q}_{1/2}/c)$ for various system sizes. It is important to note, first of all, that the values are quite accurate already for very small system sizes and, second of all, that we do not have to compare systems of different lengths. These two properties make this analysis very powerful, also for systems for which we do not know what the continuum limit is.

Table 4.4: In this table we summarize the values we extract from the parabola fits for $E_{1/2}/c$ and $\tilde{Q}_{1/2}/c$ for various system sizes. Note that for each chain length we give two pairs of extracted values. They correspond to two different highest weight states in the Neveu-Schwarz sector. Furthermore, the values are extracted from two different fits, namely a fit to the flow of that particular highest weight state to the Ramond sector. To be precise, for the chains with length $L = 3j$ the middle two columns are extracted from a fit to the flow of state 1 in figure 4.4(e) to state 7 in figure 4.4(f), whereas the last two columns are extracted from a fit to the flow of state 2 in figure 4.4(e) to state 8 in figure 4.4(f). For the chains with length $L = 3j + 1$ the middle two columns are extracted from a fit to the flow of state 1 in figure 4.4(a) to state 6 in figure 4.4(b), and the last two columns are extracted from a fit to the flow of state 2 in figure 4.4(a) to state 7 in figure 4.4(b). For the chains with length $L = 3j - 1$ the middle two columns are extracted from a fit to the flow of state 1 in figure 4.4(c) to state 7 in figure 4.4(d), and the last two columns are extracted from a fit to the flow of state 3 in figure 4.4(c) to state 6 in figure 4.4(d).

chain length	fermion number	$E_{1/2}/c$ from first fit	$\tilde{Q}_{1/2}/c$ from first fit	$E_{1/2}/c$ from second fit	$\tilde{Q}_{1/2}/c$ from second fit
6	2	-0.085	-0.004	0.339	0.846
9	3	-0.084	-0.002	0.285	0.738
12	4	-0.084	-0.001	0.270	0.706
15	5	-0.084	-0.001	0.263	0.692
18	6	-0.084	0.000	0.259	0.685
21	7	-0.083	0.000	0.257	0.680
24	8	-0.083	0.000	0.255	0.677
27	9	-0.083	0.000	0.254	0.675
5	2	0.086	0.338	0.138	-0.560
8	3	0.084	0.335	0.101	-0.407
11	4	0.084	0.334	0.093	-0.372
14	5	0.084	0.334	0.089	-0.357
17	6	0.084	0.334	0.087	-0.350
20	7	0.083	0.334	0.086	-0.346
23	8	0.083	0.334	0.086	-0.343
26	9	0.083	0.334	0.085	-0.341
7	2	0.085	0.336	0.108	-0.436
10	3	0.084	0.335	0.095	-0.381
13	4	0.084	0.334	0.09	-0.362
16	5	0.084	0.334	0.088	-0.352
19	6	0.084	0.334	0.087	-0.347
22	7	0.083	0.334	0.086	-0.344
25	8	0.083	0.334	0.085	-0.342

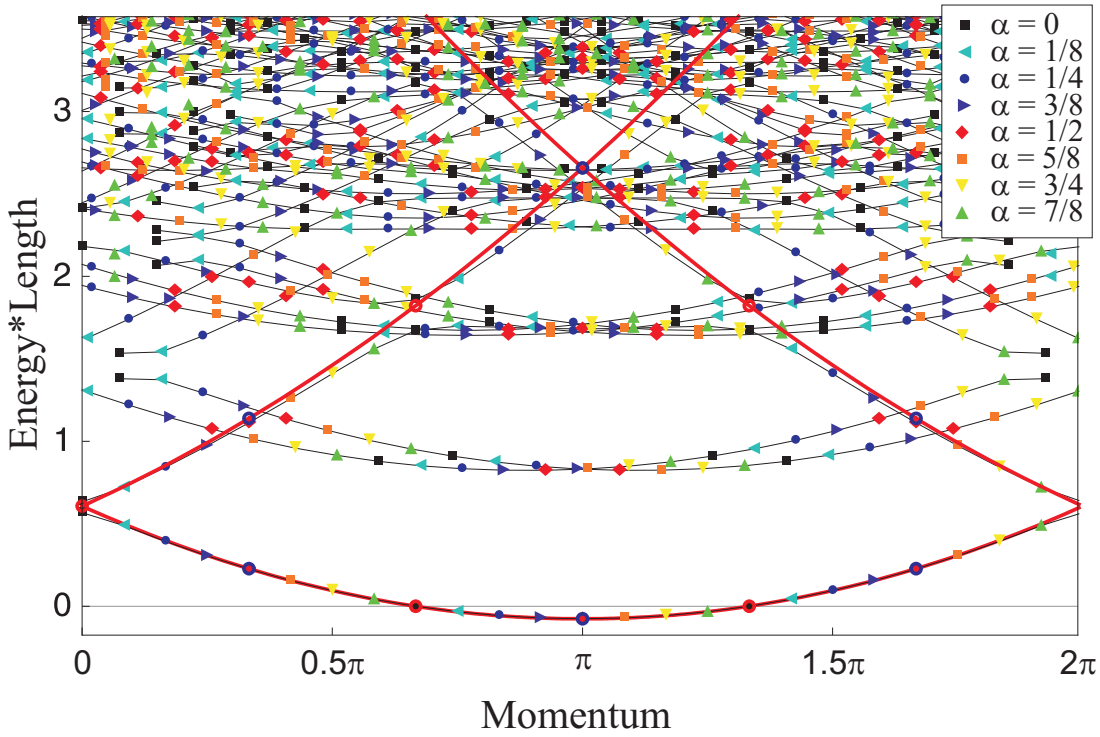

Figure 4.6: We show the spectra (energy times chain length versus momentum) of the 27-site periodic chain with 9 fermions for $\alpha = 0, \frac{1}{8}, \frac{1}{4}, \frac{3}{8}, \frac{1}{2}, \frac{5}{8}, \frac{3}{4}, \frac{7}{8}$. It follows that the spectrum given by the black squares is precisely the spectrum plotted in figure 4.4(e) and the spectrum given by the red diamonds is also plotted in figure 4.4(f). The black line connects the levels for different values of the twist parameter. The red line is the parabola obtained from a fit to the flow of one of the Ramond vacua (state 1 in figure 4.4(e)) to the Neveu-Schwarz vacuum (state 7 in figure 4.4(f)). The open red (blue) circles on this parabola correspond to $\alpha = 0 \mod 1$ ($\alpha = 1/2 \mod 1$). The two lowest energy states follow the parabola very nicely as a function of the twist parameter. For the higher energy states, we see that there are avoided level crossings (see also the end of section 4.7.7) at integer values of α, but for intermediate values of α they still qualitatively follow the parabola. By eye one can also clearly distinguish the parabola's through the first descendants of the Neveu-Schwarz vacuum, again interrupted by occasional avoided crossings.

4.9 Open boundary conditions

In the previous sections, we have discussed the continuum limit of the supersymmetric model on the periodic chain in great detail. In this section we will discuss the chain with open boundary conditions. We will first identify the continuum theory (the $\mathcal{N} = 2$ superconformal field theory at $c = 1$) and the three sectors corresponding to the three possible chain lengths modulo three. In the second part, we discuss some results by Beccaria and De Angelis [51] on one-point functions in the chain with open boundary conditions.

4.9.1 Continuum theory

In the previous sections, we have discussed the continuum limit of the supersymmetric model on the periodic chain in great detail. In this section we will discuss the chain with

open boundary conditions. A first guess is that the open boundary conditions couple the left- and right-moving modes, so that the continuum field theory becomes the $\mathcal{N} = 2$ superconformal field theory with central charge $c = 1$. By comparing the spectrum of this theory with numerical computations of finite size spectra, we concluded that this is indeed the correct guess. Let us first discuss the $\mathcal{N} = 2$ superconformal field theory with central charge $c = 1$ in some detail.
The states of the field theory are given by the vertex operators

$$V_m = e^{(\imath m\Phi/\sqrt{3})}, \tag{4.61}$$

where the $\sqrt{3}$ comes from the compactification radius $R = \sqrt{3}$ and $m \in Z$ in the Neveu-Schwarz sector and $m \in Z + 1/2$ in the Ramond sector. The conformal dimension h_m corresponding to V_m is

$$h_m = m^2/6. \tag{4.62}$$

For $m = \pm 3$ we find the supercharges, given by

$$G^{\pm} = e^{(\pm\imath\sqrt{3}\Phi)}, \tag{4.63}$$

with conformal dimension $h = 3/2$.
In the following we only consider the Ramond sector, since this is the sector that is realized in the lattice model. There are three highest weight states that we need to consider. They correspond to the primary fields: $V_{-1/2}$, $V_{1/2}$ and $V_{3/2}$. All other states are generated by the supercharges and the Virasoro algebra. The fields $V_{-1/2}$ and $V_{1/2}$ both have conformal dimension $h = 1/24$. Since the hamiltonian is given by $H = L_0 - c/24$, they correspond to zero energy states. The state $V_{3/2}|0\rangle$, however, has energy $E = 9/24 - 1/24 = 1/3$ and also has a superpartner $(V_{-3/2}|0\rangle)$.
Since the supercharges change m by ± 3, we infer that $m/3$ corresponds to the fermion number in the lattice model. It thus quickly follows that the three sectors; $m = 1/2, 3/2, 5/2 \mod 3$, are related to the three sectors in the lattice model with chain lengths $L = 0, 1, 2 \mod 3$. Indeed from section 4.4, we know that chains of length $L = 0, 2 \mod 3$ have one zero energy ground states and chains of length $L = 1 \mod 3$ have all energies larger than zero. It follows that chains with length $L = 1 \mod 3$ correspond to the sector with $m = 3/2 \mod 3$. To identify the sector of the other two chain lengths, we look at the first excited state and its superpartner. The first excited state is given by $L_{-1}V_{\pm 1/2}|0\rangle$ and the respective superpartners are $G^{\mp}_{-1}V_{\pm 1/2}|0\rangle = V_{\mp 5/2}|0\rangle$. One easily checks that the superpartners indeed have energy $E = m^2/6 - 1/24 = 1$. The difference is that one occurs at $f = f_{GS} + 1$ and the other at $f = f_{GS} - 1$. If we compare this with the finite size spectra we quickly conclude that open chains with length $L = 3j$ correspond to the sector with $m = 5/2 \mod 3$ and chains with length $L = 3j - 1$ correspond to the sector with $m = 1/2 \mod 3$.
Finally, we find the following relation between fermion number f, chain length L and the quantum number m:

$$\tilde{f} \equiv f - L/3 = (m + 1/2)/3. \tag{4.64}$$

For $m = -1/2$ this relation gives $\tilde{f} = 0$, which agrees with $f = j$ and $L = 3j$. For $m = 1/2$ this relation gives $\tilde{f} = 1/3$, which agrees with $f = j$ and $L = 3j - 1$. Finally, for $L = 3j + 1$ the two lowest energy states are found at $f = n$ and $f = n + 1$, which matches with $m = -3/2$ and $m = 3/2$.

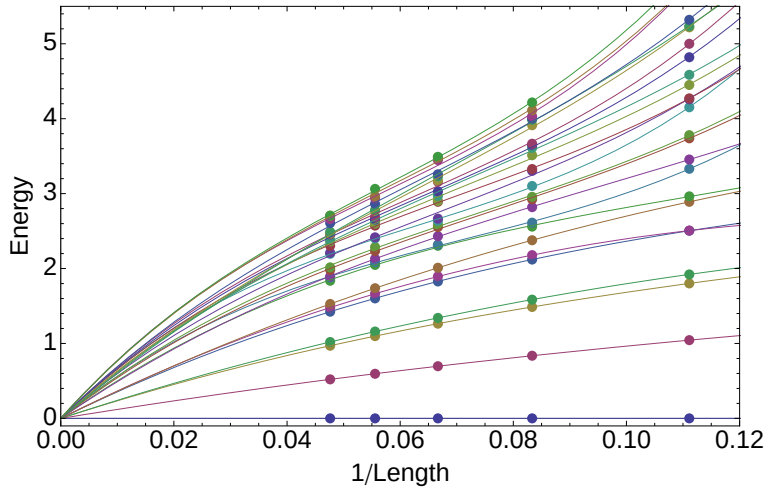

Figure 4.7: The numerically obtained energies are plotted against the inverse chain length. The fits are obtain by fitting the function $f(L) = a/L + b/L^2 + c/L^3$. The energy in the continuum limit then follows from $E = a/(\pi v_F)$.

Table 4.5: The degeneracy at level n is given by the number of partitions $p(n)$. The energy at level n is given by $E = m^2/6 - 1/24 + n$.

level	0	1	2	3	4	5	6	7	8	9	10	11	12
degeneracy	1	1	2	3	5	7	11	15	22	30	42	56	77

The spectrum per sector now simply follows from the highest weight states and their descendants. The character formula is given by (see 4.42)

$$\begin{aligned} \chi_h(q) &= q^h/\eta(q) \\ &= q^{m^2/6}/\eta(q). \end{aligned} \tag{4.65}$$

From this formula we obtain the degeneracies at each level. For the first few levels the degeneracies are summarized in the table below (Tab. 4.5). The energy of the n-th level is given by $E = m^2/6 - 1/24 + n$. The spectra are plotted for the three different sectors in figures 4.8(a), 4.9(a) and 4.10(a).
We now compare the theory explained above to the numerics. We perform a scaling analysis for the numerically obtained energies for chains of lengths up to $L = 23$. The low lying levels are nicely fitted with the function $f(L) = a/L + b/L^2 + c/L^3$. As an example we show the raw data and the fits for chain lengths $L = 3j$ and fermion number $f = j$ in figure 4.7. For open boundary conditions the scaling is given by

$$E_{\text{num}} = \pi E_{\text{SCFT}} v_F / L + \mathcal{O}(1/L^2), \tag{4.66}$$

where the Fermi velocity is given by $v_F = 9\sqrt{3}/4$. It follows that the energies in the continuum limit can be extracted from the fits via $E = a/(\pi v_F)$. The continuum limit spectra that we extracted in this way for the various chain lengths $L = 0, 1, 2 \mod 3$ are plotted in figures 4.8(b), 4.9(b) and 4.10(b). Clearly, for the first few levels, we find a very nice agreement with the theoretically obtained spectra. For the higher levels, the fits are not very reliable. We indicate two reasons for this. First of all, there is a large degeneracy

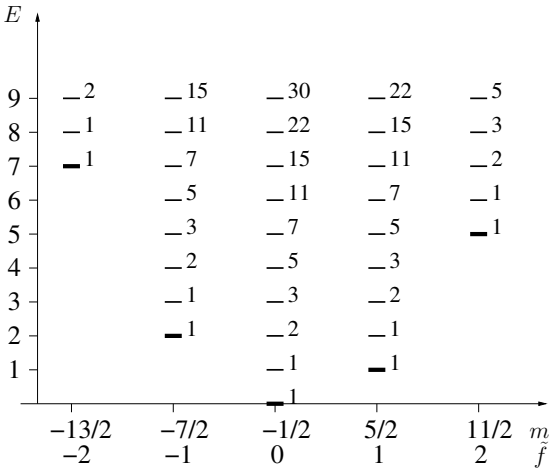

(a) The energy levels $E = m^2/6 - 1/24 + n$ are plotted versus m for $m = 5/2 \mod 3$ which corresponds to chains of length $L = 3j$. On the horizontal axis we also indicate the shifted fermion number $\tilde{f} \equiv f - L/3 = (m + 1/2)/3$. The level corresponding to the highest weight state and the levels that are generated from this field by the supercharge operators, that is the levels with energy $E = m^2/6 - 1/24$, are indicated by a thick bar. The descendants are indicated by thinner bars. The labels indicate the degeneracy of the levels.

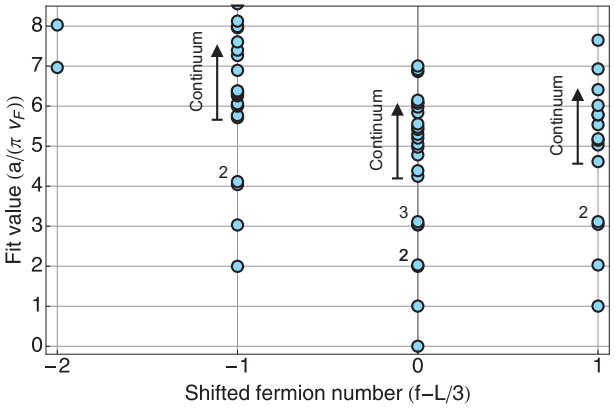

(b) The numerically fitted values of the energy are plotted versus the shifted fermion number $\tilde{f} \equiv f - L/3$ for chains of length $L = 3j$. The fit values are obtained by fitting the numerically obtained energies as a function of the chain length L with the function $f(L) = a/L + b/L^2 + c/L^3$. The energy is then given by $E = a/(\pi v_F)$. The labels indicate the number of overlapping data points.

Figure 4.8: On the left we show the theoretically predicted spectrum and on the right the spectrum obtained from fits to the numerically obtained spectra. These spectra are for chains of length $L = 3j$.

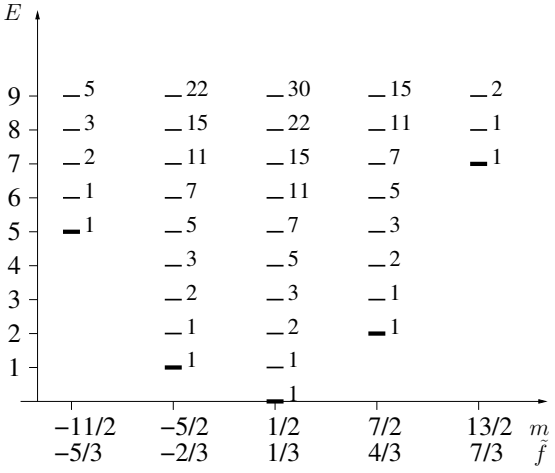

(a) The energy levels E are plotted versus m and $\tilde{f}$ for $m = 5/2 \mod 3$ which corresponds to chains of length $L = 3j - 1$.

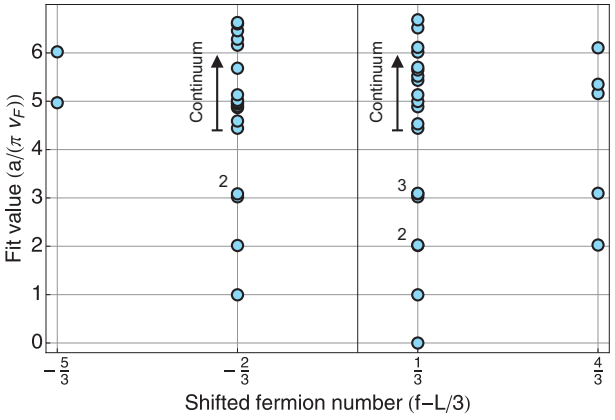

(b) The numerically fitted values of the energy are plotted versus the shifted fermion number $\tilde{f} \equiv f - L/3$ for chains of length $L = 3j - 1$.

Figure 4.9: On the left we show the theoretically predicted spectrum and on the right the spectrum obtained from fits to the numerically obtained spectra. These spectra are for chains of length $L = 3j - 1$.

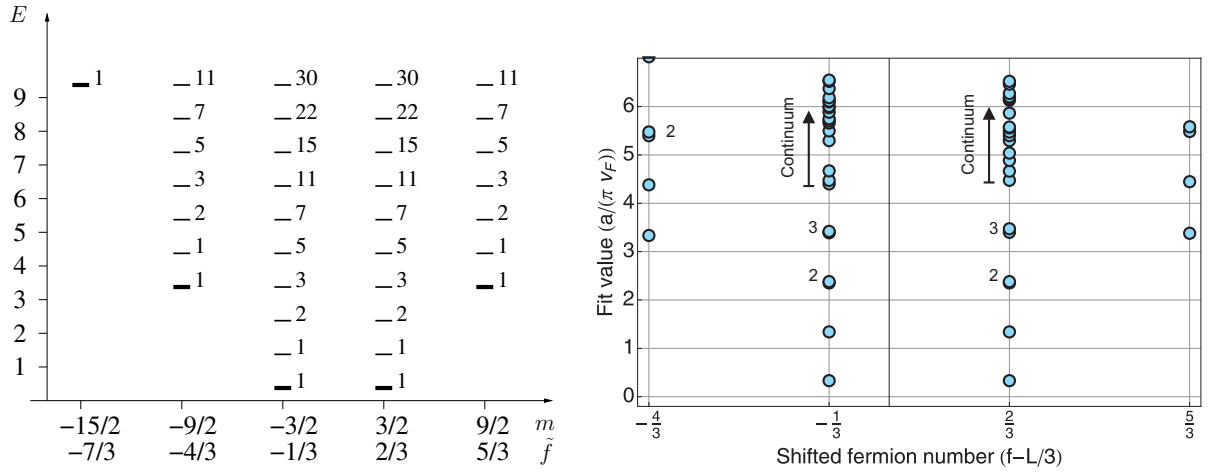

(a) The energy levels E are plotted versus m and $\tilde{f}$ for $m = 5/2 \mod 3$ which corresponds to chains of length $L = 3j + 1$.

(b) The numerically fitted values of the energy are plotted versus the shifted fermion number $\tilde{f} \equiv f - L/3$ for chains of length $L = 3j + 1$.

Figure 4.10: On the left we show the theoretically predicted spectrum and on the right the spectrum obtained from fits to the numerically obtained spectra. These spectra are for chains of length $L = 3j + 1$.

of these levels in the continuum limit. However, in the finite size spectra the degeneracies are not realized, since for finite size matrices the eigenvalues tend to spread. Second of all, since there are corrections of order $1/L^p$ with $p \geq 2$, there can be level crossings as a function of the length. Numerically, however, we simply connect the n-th level at different lengths, so we do not take possible level crossings into account. The latter argument also explains why supersymmetry may appear to be broken in the spectra extracted from the fits. Clearly, this is not the case in the original numerical spectra.
Using density renormalization group methods, one can obtain the low lying levels for much larger system sizes. In figure 4.11 we show the spectrum for the 120-site chain with open boundary conditions [66]. The spectrum and level degeneracies are, at least up to level 7, in excellent agreement with the continuum theory in the sector with $m = -1/2 \mod 3$.

4.9.2 One-point functions

In [51] Beccaria and De Angelis discuss the supersymmetric model on the chain with open boundary conditions and length $L \mod 3 = 0$. In particular, they use non standard number theoretical methods to obtain exact expressions for the ground state wave function, on the one hand, and on the other hand, they study the finite size scaling behavior of some simple correlation functions using exact diagonalization. In this section we present and interpret their results for the one point-function $\langle n_k \rangle = \langle \psi_0 | c_k^\dagger c_k | \psi_0 \rangle$. Their results can be summarized as follows. They find that $\langle n_k \rangle$ has a clear $\mathbb{Z}_3$ substructure. The one-point functions $\langle n_{k,k=1 \mod 3} \rangle$ and $\langle n_{k,k=0 \mod 3} \rangle$ are not symmetric under $k \mapsto L - k$. The one-point function $\langle n_{k,k=2 \mod 3} \rangle$ *is* symmetric under this map, however, it shows a very different behavior from the other two. For the different branches they extract the following finite size scaling behavior

- $\langle n_k \rangle - 1/3 = f_+ \left((k - k_+)/\tilde{L} \right) \tilde{L}^{-\nu}$ for $k \mod 3 = 2$,

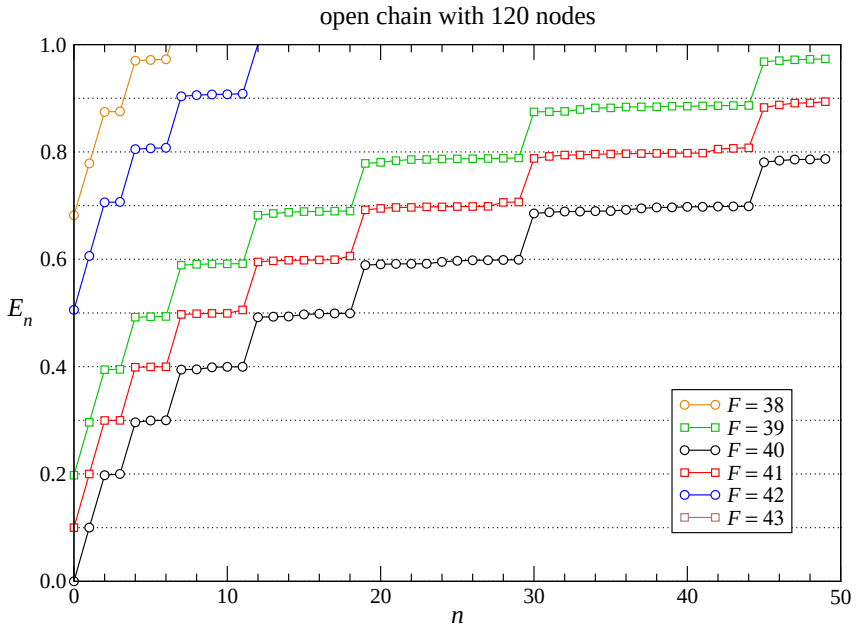

Figure 4.11: We show the spectrum of an open chain with 120 sites obtained by Campostrini [66] using DMRG methods. The energy is plotted as a function of the level number for the different fermion numbers. The different curves correspond to different fermion numbers. It is easily verified that, at least up to level 7, the degeneracies are in excellent agreement with the values in the field theory in the sector with $m = -1/2 \mod 3$ (compare with table 4.5).

- $\langle n_k + n_{k+2} \rangle - 2/3 = f_- \left((k - k_-)/\tilde{L} \right) \tilde{L}^{-\nu}$ for $k \mod 3 = 1$,

where $\tilde{L} = L/3 + 1$, $k_\pm = (L \pm 1)/2$. They obtain the best fit for $\nu = 0.33(2)$.

In the following we will use the observed $\mathbb{Z}_3$ substructure to propose an identification of the one-point functions and expectation values of operators in the superconformal field theory on the strip. We show how these expectation values can be computed analytically by mapping the strip onto the plane and introducing the mirror images to ensure the boundary conditions are preserved. The formulae we obtain are in nice agreement with the finite size scaling behavior found in [51].

Let us first identify the $\mathbb{Z}_3$ operator in the superconformal field theory on the strip. Remember that the boson is compactified: $\Phi \equiv \Phi + 2\pi R$, with $R = \sqrt{3}$. It follows that the operator T that acts as follows $T : \Phi \mapsto \Phi + 2\pi\sqrt{3}/3$ satisfies $T^3 = 1$. We now consider the action of this operator on the vertex operators $V_{\pm 1} = e^{\pm \imath \Phi/\sqrt{3}}$

$$T V_{\pm 1} = e^{\pm \imath (\Phi + 2\pi\sqrt{3}/3)/\sqrt{3}} = e^{\pm 2\pi \imath/3} V_{\pm 1}. \tag{4.67}$$

Furthermore, we trivially have $T V_0 = V_0$ and clearly V_0 is just the identity. It follows that V_0 and $V_{\pm 1}$ are eigenfunctions of the $\mathbb{Z}_3$ operator with eigenvalues $\omega_0 = 1$ and $\omega_{\pm 1} = e^{\pm 2\pi\imath/3}$ respectively.

In the lattice the one-point function $\langle n_k \rangle$ shows strong oscillations with period three in k. It follows that we can identify the inverse translation operator which sends k to $k - 1$

as the $\mathbb{Z}_3$ operator[1]. We thus find that the functions,

$$\omega_l^{-1} n_{k-1} + n_k + \omega_l n_{k+1}, \tag{4.68}$$

are eigenfunctions of the inverse translation operator with eigenvalues $\omega_l = e^{2\pi\imath l/3}$. In the following, we will assume[2] $k \mod 3 = 2$.
Combining these observations we find

$$\begin{aligned} A_0 V_0 &= n_{k-1} + n_k + n_{k+1} \\ A_1 V_{\pm 1} &= e^{\mp 2\pi\imath/3} n_{k-1} + n_k + e^{\pm 2\pi\imath/3} n_{k+1}, \end{aligned}$$

where A_0 and A_1 are constants. From the fact that the ground state has filling $1/3$, we immediately find that $A_0 = 1$. Solving the above equations for the n_k we obtain

$$\begin{aligned} 3n_k &= V_0 + A_1(V_1 + V_{-1}) \\ 3n_{k+1} &= V_0 + A_1(e^{-2\pi\imath/3} V_1 + e^{2\pi\imath/3} V_{-1}) \\ 3n_{k-1} &= V_0 + A_1(e^{2\pi\imath/3} V_1 + e^{-2\pi\imath/3} V_{-1}). \end{aligned}$$

Now we wish to compute the expectation values of these operators. To do that however, we have to map the strip onto the plane, where the correlator of vertex operators $V_\alpha = \exp(\pi\imath\alpha\Phi)$ gives

$$\langle V_{\alpha_1}(z_1) V_{\alpha_2}(z_2) \dots V_{\alpha_n}(z_n) \rangle = \prod_{i<j} (z_i - z_j)^{\alpha_i \alpha_j}. \tag{4.69}$$

To illustrate how we go from the strip to the plane we compute the expectation value of the vertex operator $V_1 = e^{\pi\imath\Phi/\sqrt{3}}$ in the Neveu-Schwarz vacuum. To compute this we have to do two steps. First we extend the strip of length L to a cylinder with radius $2L$, where we use the image-technique to ensure that the boundary conditions are unchanged. Then we use a conformal map to map the cylinder onto the complex plane, where we can compute the expectation value. The first step gives

$$\langle 0|V_1(x)|0\rangle_{\text{strip}} = \langle 0|V_1(x) V_{-1}(2L - x)|0\rangle_{\text{cyl}}, \tag{4.70}$$

where the image of $V_1(x)$, $V_{-1}(2L - x)$, is included when going from the strip of length L to the cylinder with radius $2L$. The two-point function is an equal time correlator, so the coordinates on the cylinder are $u_1 = x + \imath t$ and $u_2 = 2L - x + \imath t$. Mapping the cylinder to the plane we get $z = e^{\pi\imath u/L}$. We thus find

$$\begin{aligned} \langle 0|V_1(x) V_{-1}(2L - x)|0\rangle_{\text{cyl}} &= \left(\frac{\partial z_1}{\partial u_1}\right)^{h_1} \left(\frac{\partial z_2}{\partial u_2}\right)^{h_2} \langle 0|V_1(z_1) V_{-1}(z_2)|0\rangle_{\text{plane}} \\ &= \left(\frac{\pi\imath}{L} z_1\right)^{1/6} \left(\frac{\pi\imath}{L} z_2\right)^{1/6} (z_1 - z_2)^{-1/3} \\ &= \left(\frac{\pi\imath}{L}\right)^{1/3} \left(e^{\pi\imath(u_1+u_2)/L}\right)^{1/6} \left(e^{\pi\imath u_1/L} - e^{\pi\imath u_2/L}\right)^{-1/3} \\ &= \left(\frac{\pi\imath}{L}\right)^{1/3} \left(e^{-2\pi t/L}\right)^{1/6} e^{-\pi t/3L} \left(e^{\pi\imath x/L} - e^{\pi\imath(2L-x)/L}\right)^{-1/3} \\ &= \left(\frac{\pi}{2L}\right)^{1/3} \sin^{-1/3}(\pi x/L). \end{aligned}$$

[1] Note that there is an ambiguity here: we could just as well have identified the translation operator, which sends k to $k + 1$ with the $\mathbb{Z}_3$ operator. However, this ambiguity is fixed by comparison with the numerical results of [51].

[2] There is again an ambiguity here, since we could also take $k \mod 3 = 0, 1$. This choice, however, is again fixed by comparison with the numerical results of [51] (see also the end of this section).

Now remember that we identified the ground state of the chain of length $L = 3j$ and open boundary conditions with the Ramond vacuum $V_{-1/2}|0\rangle$. To compute an expectation value we define the in-state as $|R\rangle \equiv \lim_{z\to 0} V_{-1/2}(z)|0\rangle$ and the out-state as $\langle R| \equiv \lim_{z\to\infty}\langle 0|V_{1/2}(z)z^{1/12}$. These definitions ensure that

$$\begin{aligned}\langle R|R\rangle &= \lim_{z_2\to 0, z_1\to\infty}\langle 0|V_{1/2}(z_1)z_1^{1/12}V_{-1/2}(z_2)|0\rangle \\ &= \lim_{z_2\to 0, z_1\to\infty} z_1^{1/12}(z_1-z_2)^{-1/12} \\ &= 1.\end{aligned}$$

It thus follows that

$$\begin{aligned}\langle R|V_1(x)|R\rangle_{\text{strip}} &= \langle R|V_1(x)V_{-1}(2L-x)|R\rangle_{\text{cyl}} \\ &= \left(\frac{\pi\imath}{L}\right)^{1/3}(z_2z_3)^{1/6}\lim_{z_4\to 0, z_1\to\infty}\langle 0|V_{1/2}(z_1)z_1^{1/12}V_1(z_2)V_{-1}(z_3)V_{-1/2}(z_4)|0\rangle \\ &= \left(\frac{\pi\imath}{L}\right)^{1/3} z_2^{1/3}(z_2-z_3)^{-1/3},\end{aligned}$$

where $z_2 = e^{\pi\imath(x+\imath t)/L}$ and $z_3 = e^{\pi\imath(2L-x+\imath t)/L}$. In the last step we used (4.69). Equivalently we find

$$\begin{aligned}\langle R|V_{-1}(x)|R\rangle_{\text{strip}} &= \left(\frac{\pi\imath}{L}\right)^{1/3} z_3^{1/3}(z_3-z_2)^{-1/3} \\ &= \left(\frac{\pi\imath}{L}\right)^{1/3} e^{-\pi\imath/3}z_3^{1/3}(z_2-z_3)^{-1/3}.\end{aligned} \tag{4.71}$$

Combining all the above, we obtain

$$\begin{aligned}3\langle n_k\rangle &= 1 + A_1 2\left(\frac{\pi}{2L}\right)^{1/3} e^{\pi\imath/6}\frac{\cos(\pi(x-L/2)/3L)}{\sin^{1/3}(\pi x/L)} \\ 3\langle n_{k+1}\rangle &= 1 + A_1 2\left(\frac{\pi}{2L}\right)^{1/3} e^{\pi\imath/6}\frac{\sin(\pi(x-L)/3L)}{\sin^{1/3}(\pi x/L)} \\ 3\langle n_{k-1}\rangle &= 1 - A_1 2\left(\frac{\pi}{2L}\right)^{1/3} e^{\pi\imath/6}\frac{\sin(\pi x/3L)}{\sin^{1/3}(\pi x/L)}\end{aligned} \tag{4.72}$$

These equations clearly reproduce the observed scaling behavior. Comparison with the numerics suggests that we should choose $e^{\pi\imath/6}A_1 \approx 0.77$. Finally, we argue that we should identify the width of the strip L with $L_c + 3$, where L_c is the length of the chain. The way we understand this, is that the open chain can be obtained from a periodic chain with three sites extra, by pinning one particle to a certain site. Due to the hard-core character of the particles, the neighboring two sites must be empty. One thus effectively takes out three sites from the system and is left with an open chain. Finally, this implies that the sites -1 and $L_c + 2$ are identified with the boundaries of the strip: $x = 0$ and $x = L$. Consequently, an arbitrary site p of the chain should be identified with the point $x = p + 1$ on the strip. In figure 4.12(a) we show the one-point functions for a chain of length $L_c = 30$, this plot can be compared directly to the data presented in figure 1 in [51]. In figure 4.12(b) we plot the finite size scaling functions to be compared with figure 2 in [51]. The agreement with the data of Beccaria et. al. is quite convincing, however, it

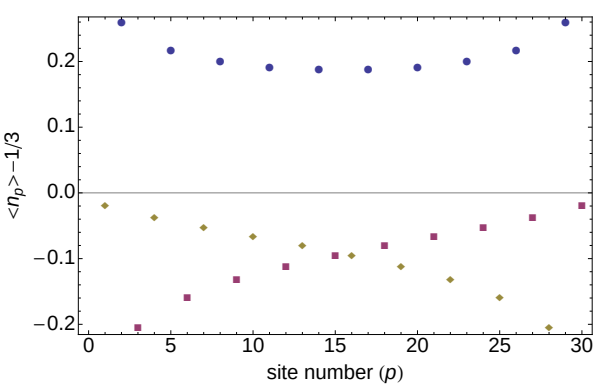

(a) One-point functions for chain length $L_c = 30$.

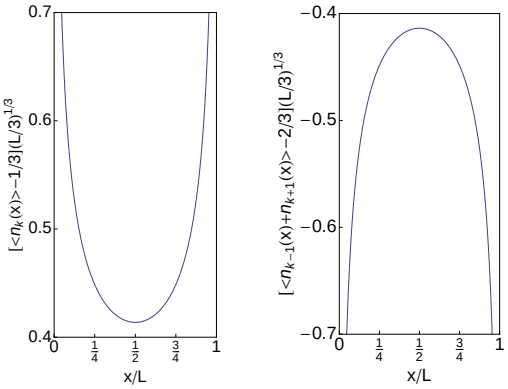

(b) Finite size scaling functions versus the normalised position on the strip (which is related to the site number, p, via $x = p + 1$).

Figure 4.12: On the left we show the one-point functions for a chain of length $L_c = 30$, this plot can be compared directly to the data presented in figure 1 in [51]. On the right we plot the finite size scaling functions, $(\langle n_k \rangle - 1/3)(L/3)^{1/3}$ and $(\langle n_{k+1} + n_{k+2} \rangle - 2/3)(L/3)^{1/3}$, to be compared with figure 2 in [51].

seems to get poorer upon approaching the boundary of the system. In particular, the value for $\langle n_1 \rangle$, which they obtain analytically using sophisticated number theoretical methods, cannot be reproduced from the field theory.

We can use the scaling functions to compute $F_i \equiv \sum_{k,k \mod 3=i} \langle n_k \rangle$, which is the average fermion number in the three branched distinguished by the site number modulo three. Replacing the sum by an integral and using that

$$\begin{aligned} \int_0^1 \frac{\cos(\pi(x-1/2)/3)}{\sin^{1/3}(\pi x)} dx &= 2^{1/3}, \\ \int_0^1 \frac{\sin(\pi x/3)}{\sin^{1/3}(\pi x)} dx &= -2^{-2/3}, \end{aligned}$$

we find

$$\begin{aligned} F_2 &= L/9 + A_1 \frac{2}{3} \left(\frac{\pi}{2L}\right)^{1/3} e^{\pi\imath/6} \frac{L}{3} 2^{1/3} \approx F/3 + 0.52\ F^{2/3}, \\ F_1 = F_0 &= L/9 - A_1 \frac{2}{3} \left(\frac{\pi}{2L}\right)^{1/3} e^{\pi\imath/6} \frac{L}{3} 2^{-2/3} \approx F/3 - 0.26\ F^{2/3}, \end{aligned}$$

where we used $e^{\pi\imath/6} A_1 \approx 0.77$ and $F = L/3$. Consequently, the oscillation in occupation number with period three in the site number, does not lead to a difference in the average fermion number in the three branches. Nevertheless, since the subleading term goes as $F^{2/3}$ it is very hard to distinguish numerically. Even for $F = 1000$ they still only differ by one order of magnitude.

On a qualitative level the $\mathbb{Z}_3$ substructure can probably be interpreted as follows. Remember that on the periodic chain we have two ground states, which are plane waves with opposite momenta differing by $2\pi/3$. It seems that for open boundary conditions these two ground states combine into a standing wave, which explains the observed density fluctuations.

An obvious follow-up on this work, is to extend it to two-point functions (see also [51]), chains of length $L \neq 0 \mod 3$ and periodic boundary conditions.

4.10 Entanglement entropy

Before closing this chapter, we wish to touch upon a last, very powerful technique to study criticality in finite size systems. Entanglement entropy is often used as a measure for the entanglement between two spatially separated parts of the system. Let ρ be the density matrix of a system in a pure quantum state $|\Psi\rangle$: $\rho = |\Psi\rangle\langle\Psi|$. Let us now divide the system in two parts A and B, such that the Hilbert space can be written as $\mathcal{H} = \mathcal{H}_A \otimes \mathcal{H}_B$ and thus $|\Psi\rangle = |\Psi_A\rangle|\Psi_B\rangle$. We then define the reduced density matrix of subsystem A as

$$\rho_A = \mathrm{Tr}_B \rho = \langle\Psi_B|\Psi\rangle\langle\Psi|\Psi_B\rangle. \tag{4.73}$$

The entanglement entropy is now defined as the Von Neumann entropy of the reduced density matrix

$$S_A = -\mathrm{Tr}\rho_A \ln \rho_A, \tag{4.74}$$

and equivalently for S_B. For a system in a pure quantum state we have $S_A = S_B$.
For a system with a gap and thus a finite correlation length, the entanglement entropy typically saturates at a certain value when the size of the subsystem exceeds a certain length related to the correlation length. For a critical system, which can be described by a conformal field theory in the continuum limit, the entanglement entropy does not saturate. In fact, it shows a universal scaling law at a conformal critical point [67, 68, 69]

$$S(l_A) = \frac{c}{3} \ln(l_A) + b, \tag{4.75}$$

where c is the central charge of the conformal field theory and b is a non-universal constant. Finally, for a one dimensional quantum critical system of finite size L, the entanglement entropy scales as [69, 70]

$$S(l_A) = \frac{c}{3} \ln(\frac{L}{\pi} \sin(\frac{l_A \pi}{L})) + b, \tag{4.76}$$

which reduces to the expression above for $L \to \infty$.
It is now clear, that if one can compute the entanglement entropy of a one dimensional system, this can be a very powerful way of studying the system. It can be used to, first of all, determine whether the system is critical or not and, second of all, if it is critical, to determine the central charge of the continuum theory. An important boundary condition for this method to work, is that one is able to determine the entanglement entropy for a subsystem larger than the correlation length if the system is gapped. For exact diagonalization this is clearly not always the case. However, if the system is studied using density matrix renormalization group (DMRG) methods [71, 72, 73], this condition is often met. Moreover, the entanglement entropy comes out essentially for free if one determines the ground state of the system with DMRG.
For the supersymmetric model on the chain, the entanglement entropy has been studied using DMRG methods [66]. The results were fitted very well by (4.76) and always in

good agreement with central charge $c = 1$ (with errors $\ll 1\%$) for the ground state of chains with periodic boundary conditions and $L = 3j \pm 1$ or with anti-periodic boundary conditions and $L = 3j$. As can be seen from figure 4.4, the ground state for the other cases, that is periodic boundary conditions and $L = 3j$ or anti-periodic boundary conditions and $L = 3j \pm 1$, is degenerate. To determine the central charge reliably in these cases one would have to construct translational invariant ground states. Finally, for the chain with open boundary conditions it is difficult to obtain a precise determination of the central charge since the entanglement entropy is plagued by very strong oscillations of period 3. Clearly, these oscillations are strongly related to the oscillations in the fermion number densities (see section 4.9.2).
Using exact diagonalization, we determined the entanglement entropy for the ground state of chains with periodic boundary conditions and $L = 3j \pm 1$, for L up to 23. The systems are too small to get a good determination of the central charge. They are, however, in reasonable agreement with $c = 1$. Excluding the values for $l_A < 3$ and $l_A > L - 3$, we obtain $c \approx 1.05$ for $L = 22$ and $c \approx 1.04$ for $L = 23$ (see figure 4.13).

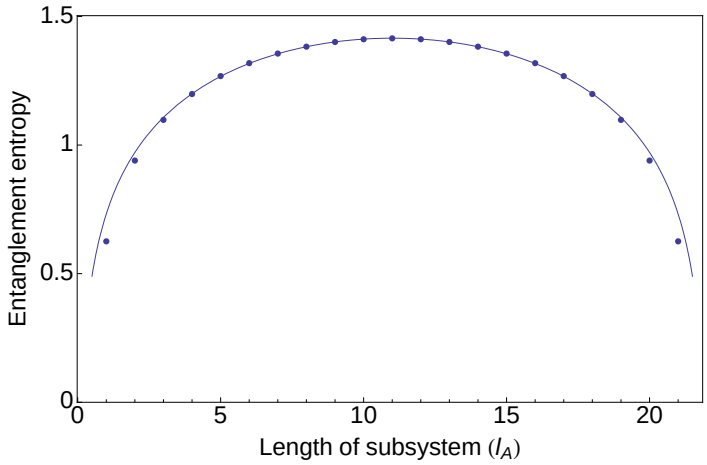

(a) $L = 22$ and $f = 7$.

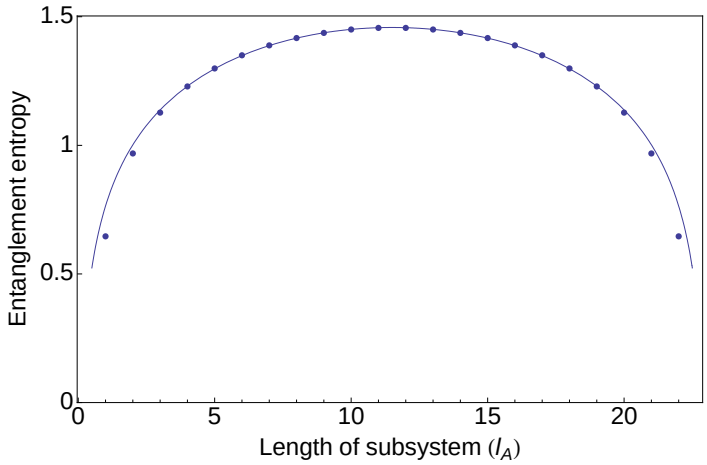

(b) $L = 23$ and $f = 8$.

Figure 4.13: Entanglement entropy versus subsystems size l_A for the ground state of the chain of length $L = 22$ with $f = 7$ fermions (left) and the chain of length $L = 23$ with $f = 8$ fermions (right).